

NISTIR 5384

**COMBINED BUOYANCY- AND PRESSURE-
DRIVEN FLOW THROUGH A
HORIZONTAL VENT**

Leonard Y. Cooper

April 1994
Building and Fire Research Laboratory
National Institute of Standards and Technology
Gaithersburg, MD 20899



U.S. Department of Commerce
Ronald H. Brown, *Secretary*
Technology Administration
Mary L. Good, *Under Secretary for Technology*
National Institute of Standards and Technology
Arati Prabhakar, *Director*

TABLE OF CONTENTS

	<u>Page</u>
TABLE OF CONTENTS	iii
LIST OF TABLES	v
LIST OF FIGURES	vi
ABSTRACT	1
INTRODUCTION	2
THE STANDARD VENT-FLOW MODEL AND ITS SHORTCOMINGS	3
Anomaly of the Standard Model for Horizontal Vents Near $\Delta p = 0$; the Mixed Flow Regime	3
The Uni-directional Flow Regime and the Significant Dependence of C_D on Relative Buoyancy	4
Representing Flow Rates as Explicit Function of Δp	6
THEORETICAL CONSIDERATIONS OF THE FLOW DYNAMICS FOR UNSTABLE CONFIGURATIONS	6
The Boundary Value Problems	6
THE DIMENSIONLESS VOLUME FLOW RATES	8
UNI-DIRECTIONAL FLOW	9
The Flow Coefficient and the Large-Grashof Number Assumption	9
The Flooding Condition	10
An Estimate for C_D	13
The Model for the Vent Flow in the Uni-directional Flow Regime	14
THE MIXED-FLOW REGIME	15
Boundary Conditions for the Flow Components	15
Analytic Approximations for the Flow Components	15
Additional Comments Regarding Mixed-Flow Data	17
VENTCL2 - AN ALGORITHM FOR BUOYANCY-DRIVEN FLOW THROUGH HORIZONTAL VENTS	18
APPLICATIONS OF VENTCL2: STEADY BURNING IN A CEILING-VENTED ROOM	18
The Problem	19
The Relationship Between Δp and T	19
The Energy Release Rate of the Fire as a Function of T and Its Maximum Possible Value	20
Experimental Validation of the Figure 13 Solution	21
ACKNOWLEDGMENTS	22
NOMENCLATURE	23
REFERENCES	25

LIST OF TABLES

		<u>Page</u>
Table 1.	Results derived from the configuration-1 experimental data of Heskestad and Spaulding [10] for flow through a $D = 0.153\text{m}$, $L/D = 0.011$ circular vent, and from Eqs. (37) and (38') for $Fr_{\text{HIGH,FLOOD}}^{(1)}$ and $\Pi_{\text{FLOOD}}^{(1)}$	27
Table 2.	Small-L/D data on flooding conditions from Epstein and Kenton [7], Tan and Jaluria [8], and Heskestad and Spaulding [10].	28
Table 3.	$V_{\text{NET}}^{(1)}/V_{\text{HIGH,FLOOD}}^{(1)}$ vs $V_{\text{LOW}}^{(1)}/V_{\text{EX,MAX}}$ results from Epstein and Kenton [7] in the mixed flow regime for flow through circular vents or disks and tubes.	29
Table 4.	Data on ceiling-vented wood fire scenarios (Jansson, Onnermark, and Halvarsson [19]) and application of Figure 13 and Eqs. (70) and (71).	30

LIST OF FIGURES

	<u>Page</u>
Figure 1.	The basic horizontal-vent configuration. 31
Figure 2.	(a) Configuration 1 and (b) Configuration 2 illustrating conditions associated with boundary value problems 1 and 2, respectively. 32
Figure 3.	Plot of $\bar{Fr}_{HIGH,FLOOD}^{(N)}$ as a function of Gr for all small-L/D data of Table 2 (O - Epstein and Kenton [7]; Δ - Tan and Jaluria [8]; \square - Heskestad and Spaulding [10]). . . 33
Figure 4.	Plot of $\bar{Fr}_{HIGH,FLOOD}^{(1)}(\epsilon)$: data of Table 2 (O - Epstein and Kenton [7], \square - Heskestad and Spaulding [10]); —, least-squares curve fit of Eq. (37). . . . 34
Figure 5.	Plot of the $\Pi_{FLOOD}^{(1)}(\epsilon)$: data of Table 2; —, least-squares curve fit of Eq. (38'). 35
Figure 6.	Plot of $C_{D,FLOOD}^{(1)}(\epsilon)$: \square , data of Table 2; —, curve fit of Eq. (39). 36
Figure 7.	Plot of $C_D^{(1)}/C_{D,\infty}$ vs $\bar{Fr}_{HIGH}^{(1)}/\bar{Fr}_{HIGH,FLOOD}^{(1)}$: —, Eq. (44) and (45); \blacksquare , non-flooding data of Table 1; \square , flooding data of Table 1. 37
Figure 8.	Plot of $\dot{V}_{HIGH}^{(1)}/\dot{V}_{HIGH,FLOOD}^{(1)} = \bar{Fr}_{HIGH}^{(1)}/\bar{Fr}_{HIGH,FLOOD}^{(1)}$ vs $\Delta p/\Delta p_{FLOOD}^{(1)} = \Pi/\Pi_{FLOOD}^{(1)}$: —, model equation for the uni-directional flow regime, Eqs. (45) and (46); - - -, Bernoulli flow limit of Eq. (48); \blacksquare , non-flooding data of Table 1; \square , flooding data of Table 1. 38
Figure 9.	Sketch of $\dot{V}_{HIGH}^{(1)}/\dot{V}_{HIGH,FLOOD}^{(1)}$, - - -; $\dot{V}_{LOW}^{(1)}/\dot{V}_{HIGH,FLOOD}^{(1)}$, - - -; and $\dot{V}_{NET}^{(1)}/\dot{V}_{HIGH,FLOOD}^{(1)}$ —, as functions of $\Delta p/\Delta p_{FLOOD}^{(1)}$ in the mixed flow regime. 39
Figure 10.	Plots of $\dot{V}_{LOW}^{(1)}/\dot{V}_{EX,MAX}^{(1)}$ (- - -) and $\dot{V}_{NET}^{(1)}/\dot{V}_{HIGH,FLOOD}^{(1)}$ (—) as functions of $\Delta p/\Delta p_{FLOOD}^{(1)}$ according to Eqs. (52), (53'), (54), and (57). 40
Figure 11.	Plot of $\dot{V}_{LOW}^{(1)}/\dot{V}_{EX,MAX}^{(1)}$ as a function of $\dot{V}_{NET}^{(1)}/\dot{V}_{HIGH,FLOOD}^{(1)}$ from Eqs. (52'), (53'), (54), and (57), —; Eqs. (52'), (53'), (54), and (57'), - - -; and Eq. (60), Plot of data of Epstein and Kenton [7], i.e., Table 3 (L/D = 0.0190 vent, \bullet ; L/D = 0.113 vent, \circ ; and tubes with $0.39 \leq L/D \leq 5.0$, \square). 41
Figure 12.	Configuration of a ceiling-vented room with a fire. 42
Figure 13.	Plots of $\Delta p/\Delta p_{FLOOD}$ and $\dot{Q}^* = \dot{Q}/[(1 - \psi/\psi_{AMB})\rho_{AMB}\psi_{AMB}C_{O_2}A_V^{5/2}g^{1/2}]$ as functions of T/T_{AMB} for the configuration of Figure 13. 43

COMBINED BUOYANCY- AND PRESSURE-DRIVEN FLOW THROUGH A SHALLOW, HORIZONTAL, CIRCULAR VENT

by

Leonard Y. Cooper
Center for Fire Research
National Institute of Standards and Technology
Gaithersburg, MD 20899

ABSTRACT

Combined buoyancy- and pressure-driven (i.e., forced) flow through a horizontal vent is considered where the vent-connected spaces near the elevation of the vent are filled with fluids of different density in an unstable configuration, with the density of the top space larger than that of the bottom space. With zero-to-moderate cross-vent pressure difference, Δp , the instability leads to a bi-directional exchange flow between the two spaces. For relatively large Δp , the flow through the vent is unidirectional, from the high- to the low-pressure space.

An anomaly of a standard vent flow model, which uses Δp to predict stable unidirectional flow according to Bernoulli's equation (i.e., flow-rate is proportional to $C_D \Delta p^{1/2}$, where C_D is an orifice coefficient), is discussed. Such a model does not predict the expected bi-directional flow at small-to-moderate Δp or non-zero flow at $\Delta p = 0$. Even when Δp exceeds the critical value, Δp_{FLOOD} , which defines the onset of unidirectional or "flooding" flow, it has been determined experimentally that until Δp exceeds many times Δp_{FLOOD} there is a significant dependence of C_D on the relative buoyancy of the upper and lower fluids. Also, it has been shown theoretically that the location of the high-pressure side of the vent, i.e., the top or bottom, can be expected to influence vent flow characteristics.

Previously published experimental data and results of an analysis of the relevant boundary value problems are used to develop a flow model which takes all of these effects into account. The result is a uniformly valid algorithm to calculate flow through shallow (small depth-to-span ratio), horizontal, circular vents under high-Grashof number conditions. This is suitable for general use in zone-type compartment fire models (e.g., an ambient temperature environment above the vent and a hot smokey environment below). The algorithm is used in example applications where steady rate-of-burning in a ceiling-vented room is estimated as a function of room temperature, vent area, and oxygen concentration. Results of the analysis are seen to be consistent with previously-published data involving ceiling-vented fire scenarios.

Keywords: building fires; compartment fires; computer models; fire models; mathematical models; vents; zone models

INTRODUCTION

Consider the flow through a horizontal vent where the fluids which fill the vent-connected spaces near the elevation of the vent are of arbitrary density. Assume that in each space, away from the vent, the environment is relatively quiescent with pressure well-approximated by the hydrostatic pressure field.

As in Figure 1, designate the spaces connected by the vent as top and bottom. Subscripts TOP and BOT, respectively, will always refer to conditions in these spaces near the vent elevation, but removed far enough laterally so that variations to the quiescent far-field environment of vent flows that may exist are negligible. \dot{V}_{TOP} and \dot{V}_{BOT} are the volume flow rates through the vent from top to the bottom side of the vent and from the bottom to the top side of the vent, respectively. Flow through the vent is determined by: the design of the vent, its shape and its depth, L ; the densities, ρ_{TOP} and ρ_{BOT} ; and the cross-vent pressure difference

$$\Delta p = p_{HIGH} - p_{LOW} \geq 0 \quad (1)$$

where

$$p_{HIGH} = \max(p_{TOP}, p_{BOT}); \quad p_{LOW} = \min(p_{TOP}, p_{BOT}) \quad (2)$$

Subscripts HIGH and LOW will always refer to the conditions on the high- and low-pressure sides of the vent, respectively. When $\Delta p = 0$, the HIGH/LOW designations are arbitrary. In cases where gas flows are involved, Δp is assumed to be small compared to p_{BOT} and p_{TOP} .

$$\Delta p / \bar{p} \ll 1; \quad \bar{p} = (p_{HIGH} + p_{LOW})/2 = (p_{BOT} + p_{TOP})/2 \quad (3)$$

The objective of this work is to develop a mathematical model for predicting for arbitrary specified values of p_{TOP} and p_{BOT} the rates of flow through the vent under conditions involving unstable configurations where a relatively dense fluid in the upper space overlays a less dense fluid in the lower space.

$$\Delta \rho = \rho_{TOP} - \rho_{BOT} > 0 \quad (4)$$

With zero-to-moderate Δp , the instability leads to a bi-directional exchange flow between the two spaces. As the flows enter the upper and lower spaces they are upward- and downward-buoyant, respectively, and they rise and fall as plumes to the far field. For relatively large Δp , the flow through the vent is unidirectional, from high to low pressure, with a single upward- or downward-buoyant plume.

Only quasi-steady features of the flows being studied will be discussed and analyzed. Thus, even when the flows are fluctuating it is assumed that time scales which characterize their fluctuations are relatively small i.e., it is assumed that meaningful average flow characteristics could be established, in principle, with integrals over time intervals which are relatively small compared to characteristic times of interest.

THE STANDARD VENT-FLOW MODEL AND ITS SHORTCOMINGS

There exists a simple, effective model for estimating the flow through both horizontal and vertical vents which is nearly always used in practical applications, e.g., in the modeling of compartment fire phenomena. The model, referred to here as the standard model, uses Bernoulli's equation and an orifice flow coefficient, C_D , to compute the rate of flow through the vent. For horizontal vents, Δp and, therefore, velocity are estimated to be uniform across the vent. For vertical vents, Δp varies with elevation and calculation of the flow-rate requires integration of the mass flux which varies from the top to the bottom of the vent. For vertical vents, calculation for an arbitrary vent-area shape poses no practical problem. For a rectangular vertical vent the calculation has been obtained in closed form (see, e.g., Emmons [1]). Previous use of this in room fire models is discussed by Cooper [2] and Peacock *et al* [3].

Anomaly of the Standard Model for Horizontal Vents Near $\Delta p = 0$; the Mixed Flow Regime

There is a basic problem with the standard model in the case of horizontal vents. According to this model, the flow through the vent is always unidirectional, i.e., for any Δp

$$\dot{V}_{\text{HIGH}} = \dot{V}_{\text{HIGH,ST}} = C_D A_V (2\Delta p / \rho_{\text{HIGH}})^{1/2}; \quad \dot{V}_{\text{LOW}} = \dot{V}_{\text{LOW,ST}} = 0 \quad (5)$$

where: \dot{V}_{HIGH} and \dot{V}_{LOW} are the volume flow rates through the vent from high- to the low-pressure side of the vent and from the low- to the high-pressure side of the vent, respectively; A_V is the area of the vent; and Eq. (5) provides the values of these flow rates for the standard model (indicated by the ST in the subscript).

The above flow description seems reasonable, except for one problem; namely, the prediction of a zero flow when $\Delta p = 0$. In general the prediction is wrong. To illustrate this, consider a condition of "near-zero" Δp , and assume that $\rho_{\text{TOP}} > \rho_{\text{BOT}}$, e.g., the vent joins a relatively high-temperature, small-density environment below from a relatively low-temperature, high-density environment above. This condition is one involving a state of hydrodynamic instability, where a two-directional exchange flow develops and a unidirectional description of the flow is always invalid.

The above phenomenon is illustrated by the following "bottle-emptying" experiment:

Consider a paper-capped narrow-necked bottle filled with liquid. The bottle is carefully turned upside-down and the paper is removed quickly. For this situation the standard vent-flow model predicts a zero-flow solution with the bottle remaining filled with the liquid, with a low-to-zero (vacuum) state at the top of the column of liquid in the bottle, and with $\Delta p = 0$ across the free-boundary at the vent-like mouth of the bottle. It is evident that the bottle will empty and that the zero-flow solution is not valid for this or any other unstable Figure 1 configuration.

The relevant fluid-dynamic instability for an unbounded interface has been studied by Taylor [4]. For the unstable configuration and for $\Delta p = 0$, Epstein [5] established a correlation for exchange flow rate data from salt-water/fresh-water exchange-flow experiments and Brown [6] established heat transfer correlations for analogous hot-air/cold-air exchange-flow experiments.

For any unstable arrangement of densities, if $|\Delta p|$ is small enough there will be a bi-directional or exchange flow through the vent. (This is the situation in the above bottle-emptying experiment, where there is an exchange of liquid flowing out and air flowing into the bottle at its vent-like mouth.) However, if $|\Delta p|$ is large enough the vent flow will be uni-directional. Indeed, there will always be a value $\Delta p = \Delta p_{\text{FLOOD}}$, denoted as the critical or flooding value of Δp , which separates a uni-directional or "flooding" flow

regime (for $\Delta p \geq \Delta p_{\text{FLOOD}}$) where $\dot{V}_{\text{LOW}} = 0$, from a "mixed" flow regime ($0 \leq \Delta p < \Delta p_{\text{FLOOD}}$) where $\dot{V}_{\text{LOW}} = \dot{V}_{\text{EX}} > 0$. \dot{V}_{EX} is the above-mentioned "exchange flow." Also, associated with any particular Δp_{FLOOD} value is a corresponding volumetric flooding flow rate, denoted by \dot{V}_{FLOOD} .

Epstein and Kenton [7] extended the work of Epstein [5] to non-zero Δp conditions. They studied the mixed flow regime with salt-water/freshwater experiments, measuring flow rates, but not Δp . They also acquired measurements of \dot{V}_{FLOOD} , thereby characterizing the onset of the flooding regime. Tan and Jaluria [8] carried out similar experiments, measuring Δp directly. However, the major focus of this work will be on turbulent, large Grashof number flows, and, as will be shown below, it seems that their data, acquired with relatively small-diameter ($D \leq 0.0127\text{m}$) vents, were in the laminar- or transition-flow range.

Let \dot{V}_{NET} denote the net volume flow rate through the vent from the high to the low-pressure side of the vent.

$$\dot{V}_{\text{NET}} = \dot{V}_{\text{HIGH}} - \dot{V}_{\text{LOW}} = \dot{V}_{\text{HIGH}} - \dot{V}_{\text{EX}} \geq 0 \quad (6)$$

This is defined as the forced or pressure-driven part of the vent flow. At the two extremes of the mixed flow regime, $\dot{V}_{\text{NET}} = \dot{V}_{\text{FLOOD}}$ at $\Delta p = \Delta p_{\text{FLOOD}}$ and $\dot{V}_{\text{NET}} = 0$ at $\Delta p = 0$. Similarly, \dot{V}_{EX} is the buoyancy-driven part of the flow which is zero at $\Delta p = \Delta p_{\text{FLOOD}}$ and which reaches its maximum value, $\dot{V}_{\text{EX,MAX}}$, as Δp and the forced part of the flow go to zero.

In view of the above, the standard model vent flow description of Eq. (5) must be modified as follows:

There is a mixed flow regime defined by $0 \leq \Delta p \leq \Delta p_{\text{FLOOD}}$, where $\dot{V}_{\text{LOW}} = \dot{V}_{\text{EX}} \geq 0$. In this regime

$$\dot{V}_{\text{HIGH}}(\Delta p = 0) = \dot{V}_{\text{EX,MAX}} \leq \dot{V}_{\text{HIGH}} \leq \dot{V}_{\text{HIGH}}(\Delta p = \Delta p_{\text{FLOOD}}) = \dot{V}_{\text{FLOOD}} \quad (7)$$

$$\dot{V}_{\text{LOW}}(\Delta p = \Delta p_{\text{FLOOD}}) = 0 \leq \dot{V}_{\text{LOW}} \leq \dot{V}_{\text{LOW}}(\Delta p = 0) = \dot{V}_{\text{EX,MAX}} \quad (8)$$

The Uni-directional Flow Regime and the Significant Dependence of C_D on Relative Buoyancy

In addition to the difficulties of using the standard flow model in the mixed flow regime, there is also a problem in the unidirectional flow regime. Use of a fixed value for C_D , denoted here as $C_{D,\infty}$ and associated with the orifice coefficient for high Reynolds number flows through an orifice which joins two regions of like fluids is, in general, not valid. As determined by Perry [9], $C_{D,\infty} = 0.60$ for low-mach-number flows or for incompressible fluids.

Using fire-generated hot-air/cold-air experiments and unstable horizontal vent configurations with the high pressure region on the top, it has been shown by Heskstad and Spaulding [10] that, until Δp is many times larger than Δp_{FLOOD} , there is a significant dependence of C_D on the relative buoyancy of the cross-vent environments, where $C_{D,\text{FLOOD}}$, the value of C_D at the flooding condition, was measured to only be of the order of a few tenths.

The fact that there is a difference between C_D for stable and unstable configurations should be no surprise. Consider the expected differences in characteristics of the entrance flow near the vent and their effects on C_D for flows with less-dense fluids below penetrating more-dense-fluids above (unstable) to that for flows with more-dense fluid below penetrating less-dense fluid above (stable). In the former case, the

entering fluid will tend to rise from the vent to the upper space in a buoyant plume, whereas in the latter case the entering fluid will rise to a maximum elevation, move outward and downward to the bottom of the upper space, and continue its outward movement there, away from the vent opening, as a radial "floor jet."

For "shallow" (i.e., small L/D) circular vents of length L, the data of Heskestad and Spaulding [10] (L/D = 0.011 in [10]) indicate a smooth dependence of C_D on the relative buoyancy as expressed through use of the Froude number. (In the following, the subscript HS always refers to the names of the authors of [10]) The orifice coefficients measured in [10], and other data and theoretical considerations indicate that under unidirectional flow conditions

$$C_{D,HS} = C_{D,HS}(Fr_{HS}, Gr_{HS}); \quad \lim_{Fr_{HS} \rightarrow \infty} C_{D,HS} = C_{D,\infty} \quad (9)$$

where g is the acceleration of gravity, $C_{D,\infty}$ is the large Reynolds number value of C_D typically used in the standard model, and Fr and Gr are the Froude and Grashof numbers

$$Fr_{HS} = (\dot{V}_{HIGH}/A_V)/[2gD(\rho_{TOP} - \rho_{BOT})/\rho_{TOP}]^{1/2}; \quad Gr_{HS} = g\rho_{TOP}(\rho_{TOP} - \rho_{BOT})D^3/\bar{\mu}^2 \quad (10)$$

In Eq. (10), μ is dynamic viscosity and

$$\mu = \mu(T); \quad \bar{\mu} = \mu(\bar{T}); \quad \bar{T} = (T_{TOP} + T_{BOT})/2 \quad (11)$$

where T is temperature. Although Eq. (9) indicates a general dependence of $C_{D,HS}$ on Gr_{HS} , it is noteworthy that for the range of Gr_{HS} values (of the order of 10^7) of the shallow circular-vent data acquired by Heskestad and Spaulding [10] $C_{D,HS}$ was insensitive to changes in Gr_{HS} and no systematic variation of $C_{D,HS}$ on Gr_{HS} was observed.

Beside determinations of the Fr_{HS} dependence of $C_{D,HS}$, the work of Heskestad and Spaulding [10] focused on determination of the flooding Froude number Fr_{FLOOD} , associated with measured values of \dot{V}_{FLOOD} . For shallow circular vents, these results will be seen below to augment the previously mentioned analogous results of Epstein [5].

The results of Heskestad and Spaulding [10] include limited data on each of several vent designs other than shallow circular vents. These data indicate that orifice coefficient representations analogous to Eqs. (9) and (10) can likely be established for vent designs other than shallow circular vents. In this regard, reliable results will require additional testing.

As mentioned, Heskestad and Spaulding [10] provide data in the unidirectional flow regime for unstable configurations where the high pressure is at the top of the vent. It is a major objective of this work to extend these results and to use results from Epstein [5], Epstein and Kenton [7], and Tan and Jaluria [8] to obtain a generalized model for the unidirectional and mixed flow regimes in unstable configurations where the high pressure is either at the top or the bottom.

Representing Flow Rates as Explicit Function of Δp

This paper will develop a fully-general horizontal-vent flow model for unstable configurations which removes the small- Δp anomaly of the standard model. The paper will extend a preliminary version of the model, presented and used by Cooper [2, 10] and Peacock *et al* [3], which was developed without the benefit of the results of Epstein and Kenton [7] and Heskestad and Spaulding [10]. The new model will also account for the Froude number dependence of C_D .

The objective here is to predict vent flow rates as a function of Δp . As mentioned, flow rates, but not Δp were measured in the experiments of Epstein and Kenton [7]. Therefore, in the mixed flow regime it will be necessary to use the correlated flow rate measurements of Epstein and Kenton [7] to establish the desired dependence of flow on Δp .

Similarly, for the unidirectional flow regime, a result like Eq. (9) does not provide the desired explicit dependence of flow rate on Δp . This is because the desired dependent variable, $\dot{V}_{HIGH} = \dot{V}_{HIGH,ST}$, is embedded on the right side of the first of Eq. (5) through the Fr- or \dot{V}_{HIGH} -dependence of C_D .

In developing a uniformly valid flow model, theoretical considerations of the general problem will be presented first. This will be followed by: 1) establishing an estimate for \dot{V}_{FLOOD} ; 2) developing the model for the unidirectional flow regime and the value for Δp_{FLOOD} corresponding to \dot{V}_{FLOOD} ; and 3) developing the model for the mixed flow regime.

THEORETICAL CONSIDERATIONS OF THE FLOW DYNAMICS FOR UNSTABLE CONFIGURATIONS

An unstable configuration with $p_{TOP} = p_{HIGH} > p_{BOT} = p_{LOW}$, i.e., net flow from top to bottom, will be designated as configuration 1. Similarly, an unstable configuration, but with $p_{BOT} = p_{HIGH} > p_{TOP} = p_{LOW}$, i.e., net flow from bottom to top, will be designated as configuration 2. The two configurations are sketched in Figures 2a and 2b.

The Boundary Value Problems

The boundary value problems associated with configurations 1 and 2 are identified as Problems 1 and 2, respectively. Assume that the fluid media in the top and bottom spaces are the same ideal gas. Then, in view of Eq. (3) and for the purpose of establishing the dependence of ρ on T , the equation of state for the gas can be approximated by

$$\rho T = \text{constant} = \rho_{TOP} T_{TOP} = \rho_{BOT} T_{BOT} = \bar{p}/R \quad (12)$$

where R is the gas constant and where the temperatures T_{TOP} and T_{BOT} correspond to specified ρ_{TOP} and ρ_{BOT} through Eq (12). With the constraint of Eq. (4), Eq. (12) leads to the expected result that the temperature of the gas in the bottom space, T_{BOT} , associated with the gas of relatively low density, is a relatively high temperature, etc.,

$$\Delta T = T_{BOT} - T_{TOP} > 0 \quad (13)$$

Eq. (12) will be a good approximation if

$$\Delta\rho g|X_3|/\bar{\rho} \ll 1 \text{ throughout the region of interest} \quad (14)$$

where Eq. (14) is always satisfied in practical problems, e.g., associated with ventilation of enclosed, heated/cooled spaces and with the spread of smoke (i.e., fire-heated and -contaminated air) during fires in multi-room facilities.

Designate the dependent variables velocity, pressure, density, and temperature for Problem N, $N = 1$ or 2 , as $U_i^{(N)}$, $p^{(N)}$, $\rho^{(N)}$, and $T^{(N)}$, respectively. Then, through the equations of conservation of mass, momentum (i.e., the Navier Stokes equations), energy, and the modified equation of state, Eq. (12), and for the specified parameters (which determine the boundary conditions), all of these variables are functions of the co-ordinates, $X_i^{(N)}$, and the temperature-dependent material properties: $C_p(T)$, specific heat at constant pressure; $k(T)$, thermal conductivity; and $\mu(T)$.

Problems 1 and 2 can be put in dimensionless form by introducing the dimensionless variables

Problem 1:

$$X_i^{*(1)} = X_i^{(1)}/D$$

$$U_i^{*(1)} = U_i^{(1)}/(2gD\varepsilon)^{1/2}$$

$$p^{*(1)} = (p - \bar{p} + g\bar{\rho}X_3)/(2g\Delta\rho D)$$

$$\rho^{*(1)} = (\rho/\bar{\rho} - 1)/\varepsilon$$

$$T^{*(1)} = (1 - T/\bar{T})/\varepsilon$$

Problem 2:

$$X_i^{*(2)} = X_i^{(2)}/D$$

$$U_i^{*(2)} = U_i^{(2)}/(2gD\varepsilon)^{1/2} \quad (15)$$

$$p^{*(2)} = (p - \bar{p} - g\bar{\rho}X_3)/(2g\Delta\rho D)$$

$$\rho^{*(2)} = (1 - \rho/\bar{\rho})/\varepsilon$$

$$T^{*(2)} = (T/\bar{T} - 1)/\varepsilon$$

where

$$\varepsilon = \Delta\rho/\bar{\rho} = \Delta T/\bar{T} < 2; \quad \bar{\rho} = (\rho_{\text{TOP}} + \rho_{\text{BOT}})/2 \quad (16)$$

Neglecting pdV work and viscous dissipation in the energy equation it has been shown by Cooper [12] that the dimensionless dependent variables of Eq. (15) are functions only of $X_i^{*(N)}$, ε , Π , \bar{Gr} , and \bar{Pr} where¹

$$\Pi = \Delta\rho/(4g\Delta\rho D); \quad \bar{Gr} = 2gD^3|\varepsilon|/[\mu(\bar{T})/\bar{\rho}]^2; \quad \bar{Pr} = C_p(\bar{T})\mu(\bar{T})/k(\bar{T}) \quad (17)$$

¹Since $\varepsilon > 0$, the absolute value designation for ε is unnecessary here. However it will be useful in latter applications of this equation. A similar note is relevant below in the presentation of Eqs. (47) and (51).

Thus, for example,

$$U_i^{*(N)} = U_i^{*(N)}(X_i^{*(N)}; \Pi, \varepsilon, \bar{G}r, \bar{P}r) \quad (18)$$

In addition, it has been shown by Cooper [12] that if the parameter ε is replaced by $-\varepsilon$ in Problem 1, then that problem becomes identical to Problem 2 and if the parameter ε is replaced by $-\varepsilon$ in Problem 2, then that problem becomes identical to Problem 1.

Now assume that solutions to Problems 1 and 2 exist for both negative and positive ε . Note that there is no *a priori* reason to suspect that solutions for $\varepsilon < 0$ for either problem are physically meaningful. However, because of the above-stated relationship between the $N = 1$ and 2 boundary value problems, it is evident that a general solution to one of these, including results for both positive and negative ε , provides the general solution to the physical problem of the other, i.e., for $\varepsilon > 0$. Thus, for example,

$$U_i^{*(1)}(X_i^{*(1)}; \Pi, \varepsilon, \bar{G}r, \bar{P}r) = U_i^{*(2)}(X_i^{*(2)}; \Pi, -\varepsilon, \bar{G}r, \bar{P}r) \quad (19)$$

Equations similar to Eq. (19) can also be written for the $p^{*(N)}$, $\rho^{*(N)}$, and $T^{*(N)}$. Eq. (19) will be used below as the basis for determining and extending the relationships between results of configuration 1- and 2-type experiments.

THE DIMENSIONLESS VOLUME FLOW RATES

For $N = 1$ or 2, $\dot{V}_{HIGH}^{(N)}$ and $\dot{V}_{LOW}^{(N)}$ would be calculated from

$$\dot{V}_{HIGH}^{(N)} = \int_{A_V} \sigma_{HIGH}^{(N)}(X_1^{(N)}, X_2^{(N)}, X_3^{(N)} = 0) dA_V; \quad \dot{V}_{LOW}^{(N)} = \int_{A_V} \sigma_{LOW}^{(N)}(X_1^{(N)}, X_2^{(N)}, X_3^{(N)} = 0) dA_V \quad (20)$$

$$\sigma_{HIGH}^{(N)}(U_3^{(N)}) = \begin{cases} -U_3^{(N)} & \text{where } U_3^{(N)}(X_1^{(N)}, X_2^{(N)}, X_3^{(N)} = 0) < 0 \\ 0 & \text{where } U_3^{(N)}(X_1^{(N)}, X_2^{(N)}, X_3^{(N)} = 0) \geq 0 \end{cases}$$

$$\sigma_{LOW}^{(N)}(U_3^{(N)}) = \begin{cases} U_3^{(N)} & \text{where } U_3^{(N)}(X_1^{(N)}, X_2^{(N)}, X_3^{(N)} = 0) > 0 \\ 0 & \text{where } U_3^{(N)}(X_1^{(N)}, X_2^{(N)}, X_3^{(N)} = 0) \leq 0 \end{cases}$$

For example, for unidirectional flow conditions, when $\Pi \geq \Pi_{FLOOD}$ corresponding to $\Delta p \geq \Delta p_{FLOOD}$, Eqs. (20) become

$$\dot{V}_{HIGH}^{(N)} = - \int_{A_V} U_3^{(N)}(X_1^{(N)}, X_2^{(N)}, X_3^{(N)} = 0) dA_V = -A_V \bar{U}_3^{(N)}; \quad \dot{V}_{LOW}^{(N)} = 0 \quad (21)$$

where the integral is over the entire area of the vent and $\bar{U}_3^{(N)}$ is the average value of $U_3^{(N)}$ at $X_3^{(N)} = 0$. Using Eqs. (17), the dimensionless version of Eq. (20) leads to the definition of the Froude number Fr_{HIGH} , which is a dimensionless value of \dot{V}_{HIGH} or \bar{U}_3 ,

$$\begin{aligned}\bar{Fr}_{HIGH}^{(N)} &= (\dot{V}_{HIGH}^{(N)}/A_V)/(2gD\varepsilon)^{1/2} \\ &= - [\int U_3^{*(N)}(X_1^{*(N)}, X_2^{*(N)}, X_3^{*(N)} = 0; \Pi, \varepsilon, \bar{G}r) d(A_V/D^2)] / (A_V/D^2) = - \bar{U}_3^{*(N)}\end{aligned}\quad (22)$$

Carrying out the above procedure on Eqs. (20) in a similar way for the mixed flow regime leads to

$$\begin{aligned}\bar{Fr}_{HIGH}^{(N)} &= (\dot{V}_{HIGH}^{(N)}/A_V)/(2gD\varepsilon)^{1/2} = \bar{Fr}_{HIGH}^{(N)}(\Pi, \varepsilon, \bar{G}r, \bar{P}r) \\ \bar{Fr}_{LOW}^{(N)} &= (\dot{V}_{LOW}^{(N)}/A_V)/(2gD\varepsilon)^{1/2} = \bar{Fr}_{LOW}^{(N)}(\Pi, \varepsilon, \bar{G}r, \bar{P}r)\end{aligned}\quad (23)$$

Also, using the result of Eq. (19) leads to

$$\begin{aligned}\bar{Fr}_{HIGH}^{(1)}(\Pi, \underline{+} \varepsilon, \bar{G}r, \bar{P}r) &= \bar{Fr}_{HIGH}^{(2)}(\Pi, \underline{-} \varepsilon, \bar{G}r, \bar{P}r) \\ \bar{Fr}_{LOW}^{(1)}(\Pi, \underline{+} \varepsilon, \bar{G}r, \bar{P}r) &= \bar{Fr}_{LOW}^{(2)}(\Pi, \underline{-} \varepsilon, \bar{G}r, \bar{P}r)\end{aligned}\quad (24)$$

UNI-DIRECTIONAL FLOW

The Flow Coefficient and the Large Grashof Number Assumption

The Eq. (5) definition of C_D remains useful for the uni-directional flow regime. Using Eqs. (17) and (23) in Eq. (5) leads to

$$C_D^{(N)} = [(\rho_{HIGH}/\bar{\rho})/(4\Pi)]^{1/2} \bar{Fr}_{HIGH}^{(N)}; \quad \lim_{\bar{Fr}_{HIGH}^{(N)} \rightarrow \infty} C_D^{(N)} = C_{D,\infty} \quad (25)$$

$$\rho_{HIGH}/\bar{\rho} = \begin{cases} 1 + \varepsilon/2 & \text{for } N = 1 \\ 1 - \varepsilon/2 & \text{for } N = 2 \end{cases}$$

From Eqs. (23) - (25) it follows that

$$C_D^{(N)} = C_D^{(N)}(\Pi, \varepsilon, \bar{G}r, \bar{P}r) \quad (26)$$

$$C_D^{(1)}(\Pi, \underline{+} \varepsilon, \bar{G}r, \bar{P}r) = C_D^{(2)}(\Pi, \underline{-} \varepsilon, \bar{G}r, \bar{P}r) \quad (27)$$

Note that C_D is for a particular vent design and would generally vary from one design to another, e.g., for shallow circular vents vs shallow square vents. **UNLESS NOTED OTHERWISE, THE REMAINDER OF THIS WORK FOCUSES ONLY ON TURBULENT, LARGE-GRASHOF-NUMBER FLOW THROUGH SMALL-L/D CIRCULAR VENTS**, where "small-L/D" means, approximately, $L/D < 0.10$, and where the "large Grashoff number" terminology will be clarified below.

The Flooding Condition

The region of turbulent, large- $\bar{G}r$ flow. For fixed values of ε , $\bar{G}r$, and $\bar{P}r$ there is a specific value of Π , associated with Δp_{FLOOD} and depending on N , that leads to the flooding condition. This is designated as $\Pi_{FLOOD}^{(N)}$, where

$$\Pi_{FLOOD}^{(N)} = \Pi_{FLOOD}^{(N)}(\varepsilon, \bar{G}r, \bar{P}r) = \Delta p_{FLOOD}^{(N)} / (4g\Delta\rho D) \quad (28)$$

$$\Pi_{FLOOD}^{(1)}(-\varepsilon, \bar{G}r, \bar{P}r) = \Pi_{FLOOD}^{(2)}(+\varepsilon, \bar{G}r, \bar{P}r) \quad (29)$$

and where the corresponding values $\bar{F}r_{HIGH,FLOOD}^{(N)}$, $\dot{V}_{HIGH,FLOOD}^{(N)}$, and $C_{D,FLOOD}^{(N)}$ are

$$\bar{F}r_{HIGH,FLOOD}^{(N)} = \bar{F}r_{HIGH,FLOOD}^{(N)}(\varepsilon, \bar{G}r, \bar{P}r) = \bar{F}r_{HIGH}^{(N)}(\Pi_{FLOOD}^{(N)}, \varepsilon, \bar{G}r, \bar{P}r) = (\dot{V}_{HIGH,FLOOD}^{(N)} / A_v) / (2gD\varepsilon)^{1/2} \quad (30)$$

$$C_{D,FLOOD}^{(N)} = C_{D,FLOOD}^{(N)}(\Pi_{FLOOD}^{(N)}, \varepsilon, \bar{G}r, \bar{P}r) = C_{D,FLOOD}^{(N)}(\varepsilon, \bar{G}r, \bar{P}r) \quad (31)$$

Also, from Eq. (25)

$$C_{D,FLOOD}^{(1)} = [(1 + \varepsilon/2) / (4\Pi_{FLOOD}^{(1)})]^{1/2} \bar{F}r_{HIGH,FLOOD}^{(1)} \quad (32)$$

$$C_{D,FLOOD}^{(2)} = [(1 - \varepsilon/2) / (4\Pi_{FLOOD}^{(2)})]^{1/2} \bar{F}r_{HIGH,FLOOD}^{(2)} \quad (33)$$

and from Eqs. (29) - (31)

$$\bar{F}r_{HIGH,FLOOD}^{(1)}(+\varepsilon, \bar{G}r, \bar{P}r) = \bar{F}r_{HIGH,FLOOD}^{(2)}(-\varepsilon, \bar{G}r, \bar{P}r) \quad (34)$$

$$C_{D,FLOOD}^{(1)}(+\varepsilon, \bar{G}r, \bar{P}r) = C_{D,FLOOD}^{(2)}(-\varepsilon, \bar{G}r, \bar{P}r) \quad (35)$$

In Heskestad and Spaulding [10], configuration-1 experiments with air ($\bar{P}r = 0.7$) in the uni-directional flow regime resulted in 13 sets of steady-state data. The data for each set were used to calculate $\bar{F}r$, Π , ε , and $\bar{G}r$. These are presented in Table 1. As indicated, of the 13 data points, the first 6 are associated with the flooding condition.

The results of the above theoretical analysis is for perfect gas media and is valid for the entire range $-2 < \varepsilon < 2$. However, for $|\varepsilon| \ll 1$, when the Bousinesque approximation is applicable, there is an analogy between Figure-1-type problems involving perfect gases and incompressible or nearly incompressible liquids. In the case of small- ε problems involving liquids, buoyancy effects which drive the exchange flows can be the result of temperature differences or of concentration differences of a solvent. This is the justification for use of the salt-water/fresh-water experimental data (where $|\varepsilon| < 0.2$) of Epstein and Kenton [7], Tan and Jaluria [8], and Heskestad and Spaulding [10] in the data analyses to follow.

Flooding conditions were measured in the salt-water/fresh-water experiments ($\bar{Pr} \approx 7$) of Epstein and Kenton [7] and Tan and Jaluria [8]. All small-L/D flooding data from Epstein and Kenton [7], Tan and Jaluria [8], and Heskestad and Spaulding [10] are presented in Table 2. As indicated in the table, the salt-water experiments involved both configurations 1 (referred to by Epstein and Kenton [7] as "draining" experiments) and 2 (referred to in [7] as "injection" experiments). Since Δp was not measured by Epstein and Kenton [7], Π and $C_{D,FLOOD}^{(N)}$ are not available for their data.

For all the above data, $\bar{Fr}_{HIGH,FLOOD}^{(N)}$ as a function of \bar{Gr} is plotted in Figure 3. As can be seen, for this data $\bar{Fr}_{HIGH,FLOOD}^{(N)}$ is relatively insensitive to changes in \bar{Gr} in the range $2.99(10^7) \leq \bar{Gr} \leq 2.91(10^8)$ (the data of Epstein and Kenton [7] and Heskestad and Spaulding [10]). (As will be explained below, in this range of \bar{Gr} the observed variations in $\bar{Fr}_{HIGH,FLOOD}^{(N)}$ are primarily a result of the dependence of $\bar{Fr}_{HIGH,FLOOD}^{(N)}$ on ε .) However, there is a significant increase in $\bar{Fr}_{HIGH,FLOOD}^{(N)}$, over the larger- \bar{Gr} values, for $\bar{Gr} \leq 1.42(10^7)$ (the data of Tan and Jaluria [8]). Using flooding data for square, rectangular, and circular vents, acquired over a large range of Grashof number, Figure 10 of Heskestad and Spaulding [10] indicates a similar insensitivity in flooding Froude number for the arbitrarily-large range $\bar{Gr} > 2(10^7)$ and a similar, relatively-abrupt increase in flooding Froude number as \bar{Gr} drops below approximately $2(10^7)$. (In computing \bar{Gr} here for the square- and rectangular-vent data of Heskestad and Spaulding [10], Eq. (17) is used where D is replaced by the width of the vent. Of these data, the one with the largest \bar{Gr} value, $\bar{Gr} = 1.54(10^{10})$, is for flooding flow through a rectangular vent of dimension $2.03\text{m} \times 0.91\text{m}$.)

Consistent with the above observation, it is assumed that in the present problem $\bar{Gr} > 2(10^7)$ defines a range of turbulent, buoyancy-driven, free-flow phenomena where the \bar{Gr} -dependence of the governing boundary value problem is generally negligible.

The above discussion ignores the Prandtl-number-, or \bar{Pr} -dependence of $\bar{Fr}_{HIGH,FLOOD}^{(N)}$. This is consistent with the reasonable assumption that in the large- \bar{Gr} range of practical interest, molecular diffusion effects of \bar{Pr} variations are negligible, at least for the approximate range of, say, $0.7 \leq \bar{Pr} \leq 7$ (i.e., for air and room temperature water).

In view of the above, it is assumed that for large enough \bar{Gr} , $\bar{Fr}_{HIGH}^{(N)}$, $\bar{Fr}_{LOW}^{(N)}$, and $C_D^{(N)}$ are functions of Π and ε , and $\bar{Fr}_{HIGH,FLOOD}^{(N)}$, $C_{D,FLOOD}^{(N)}$, and $\Pi_{FLOOD}^{(N)}$ are only functions of ε , i.e.,

For $\bar{Gr} > 2(10^7)$:

$$\begin{aligned} \bar{Fr}_{HIGH,FLOOD}^{(N)}(\varepsilon, \bar{Gr}, \bar{Pr}) &= \bar{Fr}_{HIGH,FLOOD}^{(N)}(\varepsilon), \text{ etc.} \\ \bar{Fr}_{HIGH}^{(N)}(\Pi, \varepsilon, \bar{Gr}, \bar{Pr}) &= \bar{Fr}_{HIGH}^{(N)}(\Pi, \varepsilon), \text{ etc.} \end{aligned} \quad (36)$$

The Eq.-(36) assumption will also be adopted below in the mixed flow regime.

Note that the above terminology, "free-flow," refers to the fact that boundary shear flows with no-slip conditions play no significant role, e.g., the flow phenomena mainly involve free jets and free plumes, and approach and exit flow dynamics near the surfaces $X_3 = 0^+$ or 0^- are not significant.

In contrast to the above, it is assumed that the range $\bar{Gr} < 2(10^7)$ defines transition and laminar flow regimes of the problem where \bar{Gr} - and possible \bar{Pr} -dependence is important.

Practical vent flow problems of the type considered here, e.g., problems related to fire safety and building ventilation, are typically confined to the large- \bar{Gr} range $\bar{Gr} > 2(10^7)$. **THE REMAINDER OF THIS WORK FOCUSES ONLY ON LARGE GRASHOF NUMBER PROBLEMS, AND, UNLESS NOTED OTHERWISE, GRASHOF- AND PRANDTL-NUMBER-INDEPENDENCE OF ALL THE FLOW PHENOMENA IS ALWAYS ASSUMED.**

The functions $\bar{Fr}_{HIGH,FLOOD}^{(N)}(\epsilon)$, $\Pi_{FLOOD}^{(N)}(\epsilon)$, and $C_{D,FLOOD}^{(N)}(\epsilon)$. The $\bar{Fr}_{HIGH,FLOOD}^{(1)}(\epsilon)$, $\Pi_{FLOOD}^{(1)}(\epsilon)$, and $C_{D,FLOOD}^{(1)}(\epsilon)$ data of Table 2 from Epstein and Kenton [7] and Heskestad and Spaulding [10] are plotted in Figures 4, 5, and 6, respectively. [The data from Tan and Jaluria [8] are not included since they do not satisfy the large- \bar{Gr} criterion of Eq. (36).] In the plots, the reciprocal properties of Eqs. (29), (34), and (35) are implemented. Thus, the data and solution are plotted in terms of the configuration 1 problem with configuration 2 results presented on the $\epsilon < 0$ side of the plot.

A least squares method was used to fit to the data of Figure 4 in the following convenient analytic form

$$\bar{Fr}_{HIGH,FLOOD}^{(1)} = 0.1754\exp(0.5536\epsilon) \quad (37)$$

and this is also plotted in Figure 4.

As seen in Figure 6, the available $C_{D,FLOOD}^{(1)}(\epsilon)$ data are very sparse with no entries for small $|\epsilon|$ or $\epsilon < 0$. Also, the scatter of the available data does not provide qualitative insight on the "shape" of the desired function. Under the circumstances and until more flooding data becomes available, it is reasonable to simply approximate $C_{D,FLOOD}^{(1)}(\epsilon)$ by a constant value. One reasonable choice for this is the average value, which is found to be 0.1830. However, since C_D is a derived property, i.e., from Eq. (5), and since the $C_{D,FLOOD}^{(1)}(\epsilon)$ entries of Table 2 are derived from the $\bar{Fr}_{HIGH,FLOOD}^{(1)}(\epsilon)$ and $\Pi_{FLOOD}^{(1)}(\epsilon)$ data according to Eq (32), it seems more appropriate that the criterion for selecting a "best," constant, representative value for $C_{D,FLOOD}^{(1)}$ is that it provides a least squares fit of the $\Pi_{FLOOD}^{(1)}(\epsilon)$ data.

From Eq. (32)

$$\Pi_{FLOOD}^{(1)}(\epsilon) = (1 + \epsilon/2)[\bar{Fr}_{HIGH,FLOOD}^{(1)}(\epsilon)/C_{D,FLOOD}^{(1)}]^2/4 \quad (38)$$

Using Eq. (37) in Eq. (38) it is found that the constant value for $C_{D,FLOOD}^{(1)}$ that provides the least squares fit to the six $\Pi_{FLOOD}^{(1)}(\epsilon)$ data points of Table 2 is

$$C_{D,FLOOD}^{(1)}(\epsilon) = 0.1780 \quad (39)$$

Eq. (28) and Eqs. (37) and (39) in (38) leads to

$$\Pi_{\text{FLOOD}}^{(1)}(\varepsilon) = \Delta p_{\text{FLOOD}}^{(1)}/(4g\Delta\rho D) = 0.2427(1 + \varepsilon/2)\exp(1.1072\varepsilon) \quad (38')$$

Eq. (38') is plotted in Figure 5 and Eq. (39) is plotted in Figure 6.

In Figure 6, the sparseness of the the available $\Pi_{\text{FLOOD}}^{(1)}(\varepsilon)$ data, especially with the absence of entries for small $|\varepsilon|$ or $\varepsilon < 0$, and the predicted significant $\Pi_{\text{FLOOD}}^{(1)}(\varepsilon)$ -variation of Eq. (38) in the ε -range of interest, is problematic. Nevertheless, the results of Eqs. (37) - (39) are plausible, and they fill a gap where alternative choices are not available. These results will be used throughout the remainder of this work.

An Estimate for C_D

It is convenient to normalize Eq. (25) as follows

$$C_D^{(1)}(\Pi, \varepsilon)/C_{D,\infty} = [C_{D,\text{FLOOD}}^{(1)}(\varepsilon)/C_{D,\infty}][\bar{F}r_{\text{HIGH}}^{(1)}(\Pi, \varepsilon)/\bar{F}r_{\text{HIGH,FLOOD}}^{(1)}(\varepsilon)]/[\Pi/\Pi_{\text{FLOOD}}^{(1)}(\varepsilon)]^{1/2} \quad (40)$$

For uni-directional flow $\Pi/\Pi_{\text{FLOOD}}^{(N)}(\varepsilon) \geq 1$ where, independent of ε , the limit $\Pi/\Pi_{\text{FLOOD}}^{(N)}(\varepsilon) \rightarrow \infty$ leads to the standard Bernoulli orifice flow condition, i.e.,

$$\lim_{\Pi/\Pi_{\text{FLOOD}}^{(1)}(\varepsilon) \rightarrow 1} C_D^{(1)}(\Pi, \varepsilon)/C_{D,\infty} = [C_{D,\text{FLOOD}}^{(1)}(\varepsilon)/C_{D,\infty}] \equiv 1/\sigma_1(\varepsilon) \quad (41)$$

$$\lim_{\Pi/\Pi_{\text{FLOOD}}^{(1)}(\varepsilon) \rightarrow \infty} C_D^{(1)}(\Pi, \varepsilon)/C_{D,\infty} = 1$$

and where $C_{D,\infty}$ is taken to be the value associated with sharp-edged orifices and slots (Perry [9])

$$C_{D,\infty} = 0.60 \quad (42)$$

In terms of reaching the objective of an estimate for vent flow rate as a function of Δp , it is convenient to choose the functional form

$$\bar{F}r_{\text{HIGH}}^{(1)}/\bar{F}r_{\text{HIGH,FLOOD}}^{(1)} = f(\Pi/\Pi_{\text{FLOOD}}^{(1)}; \varepsilon) \quad (43)$$

and to approximate $C_D^{(1)}(\Pi, \varepsilon)/C_{D,\infty}$ of Eq. (40) as

$$C_D^{(1)}(\Pi, \varepsilon)/C_{D,\infty} = c(\Pi/\Pi_{\text{FLOOD}}^{(1)}; \varepsilon) \quad (44)$$

$$= (\bar{F}r_{\text{HIGH}}^{(1)}/\bar{F}r_{\text{HIGH,FLOOD}}^{(1)})/\{[(\bar{F}r_{\text{HIGH}}^{(1)}/\bar{F}r_{\text{HIGH,FLOOD}}^{(1)}) - 1 + \sigma_2^2]^2 + \sigma_1^2 - \sigma_2^4\}^{1/2}$$

where $\sigma_2 = \sigma_2(\varepsilon)$ would be determined from a good fit of available $C_D^{(1)}(\Pi, \varepsilon)/C_{D,\infty}$ data. Note that Eq. (44) satisfies the limits of Eqs. (41).

As can be seen from Table 1, except for $\varepsilon = 0.521$, $C_D^{(1)}/C_{D,\infty}$ data for non-flooding conditions are limited to single data points for each of $\varepsilon = 0.282$ and 0.559 . Until further data are available it is therefore reasonable to approximate $\sigma_2(\varepsilon)$ as a constant.

Using Eqs. (41) and (42), and the constant- $C_{D,FLOOD}^{(1)}$ approximation of Eq. (39), and then choosing σ_2 as the constant value that provides a least squares fit to all of flooding and non-flooding data of Table 1 leads to

$$\sigma_1(\varepsilon) \approx \text{constant} = 0.60/0.1780 = 3.370; \quad \sigma_2(\varepsilon) \approx \text{constant} = 1.045 \quad (45)$$

A plot of Eq. (44) and (45) and the data of Table 1 for $C_D^{(1)}(\Pi, \varepsilon)/C_{D,\infty}$ vs $\bar{F}_{r,HIGH}^{(1)}/\bar{F}_{r,HIGH,FLOOD}^{(1)}$ is presented in Figure 7.

The Model for the Vent Flow in the Uni-directional Flow Regime

Replacing the left-hand-side of Eq. (40) by Eq. (44) and solving for $\Pi/\Pi_{FLOOD}^{(1)}$ leads to the desired result for predicting the vent flow rate in the uni-directional flow regime

for $\Delta p/\Delta p_{FLOOD}^{(1)} = \Pi/\Pi_{FLOOD}^{(1)} \geq 1$:

$$\dot{V}_{HIGH}^{(1)}/\dot{V}_{HIGH,FLOOD}^{(1)} = \bar{F}_{r,HIGH}^{(1)}/\bar{F}_{r,HIGH,FLOOD}^{(1)} = 1 - \sigma_2^2 + [\sigma_2^4 + \sigma_1^2(\Delta p/\Delta p_{FLOOD}^{(1)} - 1)]^{1/2} \quad (46)$$

$$\dot{V}_{LOW}^{(1)}/\dot{V}_{HIGH,FLOOD}^{(1)} = \bar{F}_{r,LOW}^{(1)}/\bar{F}_{r,HIGH,FLOOD}^{(1)} = 0$$

where σ_1 and σ_2 are given in Eq. (45); $\Delta p_{FLOOD}^{(1)}$ in Eq. (38'); and $\dot{V}_{HIGH,FLOOD}^{(1)}$ is found from Eqs. (30) and (37) to be

$$\dot{V}_{HIGH,FLOOD}^{(1)} = 0.1754(2gD|\varepsilon|)^{1/2}A_v \exp(0.5536\varepsilon) \quad (47)$$

From Eq. (46) it can now be seen that the functional form of Eq. (44) guarantees satisfaction of the requirement that for $\Delta p/\Delta p_{FLOOD}^{(1)} \geq 1$, $\dot{V}_{HIGH}^{(1)}/\dot{V}_{HIGH,FLOOD}^{(1)}$ is a monotonically increasing function of $\Delta p/\Delta p_{FLOOD}^{(1)}$. It can also be shown that Eq. (46) satisfies the large- Δp limit which is equivalent to the standard Bernoulli orifice flow condition, i.e.,

$$\lim_{\Delta p/\Delta p_{FLOOD}^{(1)} \rightarrow \infty} \dot{V}_{HIGH}^{(1)}/\dot{V}_{HIGH,FLOOD}^{(1)} = (C_{D,\infty}/C_{D,FLOOD}^{(1)}) (\Delta p/\Delta p_{FLOOD}^{(1)})^{1/2} \quad (48)$$

Eqs. (46) are the recommended model equations for the uni-directional flow regime. A plot of $\dot{V}_{HIGH}^{(1)}/\dot{V}_{HIGH,FLOOD}^{(1)}$ vs $\Delta p/\Delta p_{FLOOD}^{(1)}$ according to Eqs. (46) is presented in Figure 8. Included in the figure is a plot of the data of Table 1 and a plot of the Bernoulli flow limit of Eq. (48). From the figure it can be seen that at the flooding condition the standard Bernoulli flow equation would over-estimate the expected

flow rate by a factor in excess of 3, and that only after $\Delta p/\Delta p_{\text{FLOOD}}^{(1)}$ exceeds 3 or 4 does the standard-model provide flow-rate estimates which are correct to within a few tens of percent.

THE MIXED-FLOW REGIME

Boundary Conditions for the Flow Components

From Eqs. (6)-(8), $\dot{V}_{\text{HIGH}}^{(1)}/\dot{V}_{\text{HIGH,FLOOD}}^{(1)}$, $\dot{V}_{\text{LOW}}^{(1)}/\dot{V}_{\text{HIGH,FLOOD}}^{(1)}$, and $\dot{V}_{\text{NET}}^{(1)}/\dot{V}_{\text{HIGH,FLOOD}}^{(1)}$ as functions of $\Delta p/\Delta p_{\text{FLOOD}}^{(1)} \leq 1$ in the mixed flow regime are sketched in Figure 9. As indicated in the figure, in addition to the specifications of these equations it is reasonable to expect that the slopes of both $\dot{V}_{\text{HIGH}}^{(1)}/\dot{V}_{\text{HIGH,FLOOD}}^{(1)}$ and $\dot{V}_{\text{LOW}}^{(1)}/\dot{V}_{\text{HIGH,FLOOD}}^{(1)}$ are continuous across the flooding limit boundary, $\Delta p/\Delta p_{\text{FLOOD}}^{(1)} = 1$. Thus

at $\Delta p/\Delta p_{\text{FLOOD}}^{(1)} = 0$:

$$\begin{aligned}\dot{V}_{\text{HIGH}}^{(1)}/\dot{V}_{\text{HIGH,FLOOD}}^{(1)} &= \dot{V}_{\text{LOW}}^{(1)}/\dot{V}_{\text{HIGH,FLOOD}}^{(1)} = \dot{V}_{\text{EX,MAX}}/\dot{V}_{\text{HIGH,FLOOD}}^{(1)} \\ &= 0.055(4/\pi)(1/2^{1/2})/\text{Fr}_{\text{HIGH,FLOOD}}^{(1)}(\varepsilon) \\ \dot{V}_{\text{NET}}^{(1)}/\dot{V}_{\text{HIGH,FLOOD}}^{(1)} &= \dot{V}_{\text{HIGH}}^{(1)}/\dot{V}_{\text{HIGH,FLOOD}}^{(1)} - \dot{V}_{\text{LOW}}^{(1)}/\dot{V}_{\text{HIGH,FLOOD}}^{(1)} = 0\end{aligned}\tag{49}$$

at $\Delta p/\Delta p_{\text{FLOOD}}^{(1)} = 1^-$:

$$\begin{aligned}\dot{V}_{\text{HIGH}}^{(1)}/\dot{V}_{\text{HIGH,FLOOD}}^{(1)} &= \dot{V}_{\text{NET}}^{(1)}/\dot{V}_{\text{HIGH,FLOOD}}^{(1)} = 1; \quad \dot{V}_{\text{LOW}}^{(1)}/\dot{V}_{\text{HIGH,FLOOD}}^{(1)} = 0 \\ d(\dot{V}_{\text{LOW}}^{(1)}/\dot{V}_{\text{HIGH,FLOOD}}^{(1)})/d(\Delta p/\Delta p_{\text{FLOOD}}^{(1)}) &= 0 \\ d(\dot{V}_{\text{HIGH}}^{(1)}/\dot{V}_{\text{HIGH,FLOOD}}^{(1)})/d(\Delta p/\Delta p_{\text{FLOOD}}^{(1)}) &= d(\dot{V}_{\text{NET}}^{(1)}/\dot{V}_{\text{HIGH,FLOOD}}^{(1)})/d(\Delta p/\Delta p_{\text{FLOOD}}^{(1)}) \\ &= d(\dot{V}_{\text{HIGH}}^{(1)}/\dot{V}_{\text{HIGH,FLOOD}}^{(1)})/d(\Delta p/\Delta p_{\text{FLOOD}}^{(1)}) \Big|_{\Delta p/\Delta p_{\text{FLOOD}}^{(1)} = 1^+} \\ &= m_1(\varepsilon) = (\sigma_1/\sigma_2)^2/2 = 5.20\end{aligned}\tag{50}$$

where Eq. (45) was used in the last of Eq. (50), and in Eq. (49) the value of $\dot{V}_{\text{EX,MAX}}$ for shallow circular vents was obtained from Epstein [5]

$$\dot{V}_{\text{EX,MAX}} = 0.055(4/\pi)A_v(gD|\varepsilon|)^{1/2}\tag{51}$$

Analytic Approximations for the Flow Components

The following representations of $\dot{V}_{\text{NET}}^{(1)}/\dot{V}_{\text{HIGH,FLOOD}}^{(1)}$ and $\dot{V}_{\text{LOW}}^{(1)}/\dot{V}_{\text{HIGH,FLOOD}}^{(1)}$ which satisfy Eqs. (49) and (50) are adopted

$$\dot{V}_{NET}^{(1)}/\dot{V}_{HIGH,FLOOD}^{(1)} = \{M - [1 + (M^2 - 1)(1 - \Delta p/\Delta p_{FLOOD}^{(1)})^{1/2}]/(M - 1)\} \quad (52)$$

or

$$\Delta p/\Delta p_{FLOOD}^{(1)} = - [(M - 1)/(M + 1)](\dot{V}_{NET}^{(1)}/\dot{V}_{HIGH,FLOOD}^{(1)})^2 + [2M/(M + 1)](\dot{V}_{NET}^{(1)}/\dot{V}_{HIGH,FLOOD}^{(1)}) \quad (52')$$

$$\dot{V}_{LOW}^{(1)}/\dot{V}_{HIGH,FLOOD}^{(1)} =$$

$$\dot{V}_{EX,MAX}^{(1)}/\dot{V}_{HIGH,FLOOD}^{(1)} \{ [1 + m_2(\dot{V}_{HIGH,FLOOD}^{(1)}/\dot{V}_{EX,MAX}^{(1)})/2](1 - \Delta p/\Delta p_{FLOOD}^{(1)})^2 - [2 + m_2(\dot{V}_{HIGH,FLOOD}^{(1)}/\dot{V}_{EX,MAX}^{(1)})/2](1 - \Delta p/\Delta p_{FLOOD}^{(1)}) \}^2 \quad (53)$$

or

$$\dot{V}_{LOW}^{(1)}/\dot{V}_{EX,MAX}^{(1)} = [(1 + m_3/2)(1 - \Delta p/\Delta p_{FLOOD}^{(1)})^2 - (2 + m_3/2)(1 - \Delta p/\Delta p_{FLOOD}^{(1)})] \quad (53')$$

$$M = 2m_1 - 1 = (\sigma_1/\sigma_2)^2 - 1 = 9.400 \quad (54)$$

where Eq. (45) was used to obtain Eq. (54), $\dot{V}_{EX,MAX}^{(1)}/\dot{V}_{HIGH,FLOOD}^{(1)}$ is given in Eq. (49), and the yet-undetermined value for m_3 and the associated m_2 are

$$m_3(\varepsilon) = d(\dot{V}_{LOW}^{(1)}/\dot{V}_{EX,MAX}^{(1)})/d(\Delta p/\Delta p_{FLOOD}^{(1)}) \Big|_{\Delta p/\Delta p_{FLOOD}^{(1)} = 0} \quad (55)$$

$$m_2(\varepsilon) = m_3(\varepsilon) \dot{V}_{EX,MAX}^{(1)}/\dot{V}_{HIGH,FLOOD}^{(1)} = d(\dot{V}_{LOW}^{(1)}/\dot{V}_{HIGH,FLOOD}^{(1)})/d(\Delta p/\Delta p_{FLOOD}^{(1)}) \Big|_{\Delta p/\Delta p_{FLOOD}^{(1)} = 0} \quad (56)$$

Note that Eqs. (53) and (53') also satisfy the requirement that \dot{V}_{LOW} is always positive.

The Eq. (52) or (52') representation of the $\dot{V}_{NET}^{(1)}/\dot{V}_{HIGH,FLOOD}^{(1)}$ sketch of Figure 9 involves a parabola with axis parallel to the $\Delta p/\Delta p_{FLOOD}^{(1)}$ axis. This analytic form allows for the required monotonic increase of $\dot{V}_{NET}^{(1)}/\dot{V}_{FLOOD}^{(1)}$ from zero at $\Delta p/\Delta p_{FLOOD}^{(1)} = 0$ to 1 at $\Delta p/\Delta p_{FLOOD}^{(1)} = 1$. It also satisfies the large-slope requirement of the last of Eqs. (50) at $\Delta p/\Delta p_{FLOOD}^{(1)} = 1$. Finally, the representations of Eqs. (52) and (53) are in a convenient form for the curve-fitting analysis of the data of Epstein and Kenton [7], to be introduced below.

Epstein and Kenton [7] provide flow rate data for circular vents or disks ($L/D = 0.0190$ and 0.113 ; 4 data points) and tubes ($0.39 \leq L/D \leq 5.0$; 16 data points) in a limited portion of the mixed-flow regime. These are presented in Table 3. Difficulty in acquiring accurate data relatively close to the uni-directional flow regime, where $\dot{V}_{NET}^{(1)}/\dot{V}_{HIGH,FLOOD}^{(1)} > 0.6$ (indicated by the data to correspond to the portion of the mixed-flow regime where $0 \leq \dot{V}_{LOW}^{(1)}/\dot{V}_{EX,MAX}^{(1)} < 0.1$), precluded measurements of flow in this range. According to Epstein and Kenton [7], the reported data have "experimental uncertainty ... between 10 and 30 percent."

Note that all data of Table 3 are in the very narrow range $0.12 \leq \varepsilon \leq 0.16$. For this reason the data can not be used to determine any significant ε -dependence of m_3 that may exist. Accordingly, m_3 will be approximated by a constant value.

Using Eqs. (52') in (53') leads to a solution of $\dot{V}_{LOW}^{(1)}/\dot{V}_{EX,MAX}$ as a function of $\dot{V}_{NET}^{(1)}/\dot{V}_{HIGH,FLOOD}^{(1)}$. The constant value of m_3 that provides a least-squares fit of this function to the four small-L/D data pairs of Table 3 has been found to be

$$m_3 = -0.7070 \text{ (best fit for } L/D = 0.0190 \text{ and } 0.112 \text{ data of Epstein and Kenton [7])} \quad (57)$$

From Eqs. (52), (53'), (54), and (57), $\dot{V}_{LOW}^{(1)}/\dot{V}_{EX,MAX}$ and $\dot{V}_{NET}^{(1)}/\dot{V}_{HIGH,FLOOD}^{(1)}$ are plotted in Figure 10 as functions of $\Delta p/\Delta p_{FLOOD}^{(1)}$.

Using Eqs. (6) and (52)-(56), $\dot{V}_{HIGH}^{(1)}$ is finally determined from

$$\dot{V}_{HIGH}^{(1)} = \dot{V}_{NET}^{(1)} + \dot{V}_{LOW}^{(1)} \quad (58)$$

Additional Comments Regarding Mixed-Flow Data

$\dot{V}_{LOW}^{(1)}/\dot{V}_{EX,MAX}$ as a function of $\dot{V}_{NET}^{(1)}/\dot{V}_{HIGH,FLOOD}^{(1)}$ from Eqs. (52'), (53'), (54), and (57) is plotted in Figure 11. Also included is a plot of all data of Table 3. It is interesting to note that these data, the bulk of which involve flow through tube-like vents (i.e., moderate-to-large L/D) rather than shallow vents (i.e., small L/D), are well correlated by the m_3 value that was established from just the few, available, shallow-vent data.

The value of m_3 providing the least-squares fit of *all* data of Table 3 has also been determined

$$m_3 = -1.8077 \text{ (best fit for all data of Epstein and Kenton [7], } 0.0190 \leq L/D \leq 5.0) \quad (57')$$

and $\dot{V}_{LOW}^{(1)}/\dot{V}_{EX,MAX}$ as a function of $\dot{V}_{NET}^{(1)}/\dot{V}_{HIGH,FLOOD}^{(1)}$ from Eqs. (52'), (53'), (54), and (57') is also plotted in Figure 11.

It is of interest to define

$$\begin{aligned} m_4 &= \left. \frac{d(\dot{V}_{LOW}^{(1)}/\dot{V}_{EX,MAX})}{d(\dot{V}_{NET}^{(1)}/\dot{V}_{HIGH,FLOOD}^{(1)})} \right|_{\dot{V}_{NET}^{(1)}/\dot{V}_{HIGH,FLOOD}^{(1)} = \Delta p/\Delta p_{FLOOD}^{(1)} = 0} = [2m_3M/(M + 1)] \\ &= -1.2781 \text{ [using Eq. (54) and } m_3 \text{ from Eq. (57)]} \quad (59) \\ &= -2.625 \text{ [using Eq. (54) and } m_3 \text{ from Eq. (57')] } \end{aligned}$$

The latter value for m_4 can be compared to the $m_4 = -2.5$ value associated with the correlating function Eq. (24) of Epstein and Kenton [7] for all data, viz.²

$$\dot{V}_{LOW}^{(1)}/\dot{V}_{EX,MAX} = (1 - \dot{V}_{NET}^{(1)}/\dot{V}_{HIGH,FLOOD}^{(1)})^{2.5} \quad (60)$$

A plot Eq. (60) is included in Figure 11.

VENTCL2 - AN ALGORITHM FOR BUOYANCY-DRIVEN FLOW THROUGH HORIZONTAL VENTS

For unstable cross-vent densities, all of the above leads to the following algorithm, called **VENTCL2** (an advanced version of **VENTCL** (Cooper [2 and 11])), for calculating \dot{V}_{NET} , \dot{V}_{LOW} , and \dot{V}_{HIGH} through small-L/D circular vents:

1. Verify that $\rho_{TOP} > \rho_{BOT}$, i.e., that the configuration is unstable, and calculate $\Delta\rho$ from Eq. (4); determine \bar{T} from Eq. (11) and $\mu(\bar{T})$ from note {6} of Table 1; determine $\bar{\rho}$ and $\varepsilon > 0$ from Eq. (16).
2. Determine p_{HIGH} and p_{LOW} , Δp , and \bar{p} from Eqs. (1)-(3); according to Figure 1 designate the problem type as either Problem 1 or 2, involving configuration 1 or 2, respectively; if it is configuration 2, then replace ε by $-\varepsilon < 0$.
3. Determine \bar{Gr} from Eq. (17) and verify that \bar{Gr} satisfies the large- \bar{Gr} criterion, $\bar{Gr} \geq 2(10^7)$.
4. Calculate $\bar{Fr}_{HIGH,FLOOD}^{(1)}$ and then $\dot{V}_{HIGH,FLOOD}^{(1)}$ from Eqs. (37) and (47), $\Delta p_{FLOOD}^{(1)}$ from Eq. (38'), and $\Delta p/\Delta p_{FLOOD}^{(1)}$.
5. If $\Delta p/\Delta p_{FLOOD}^{(1)} \geq 1$, expect uni-directional flow. Estimate $\dot{V}_{LOW} = \dot{V}_{LOW}^{(1)} = 0$ and $\dot{V}_{HIGH} = \dot{V}_{HIGH}^{(1)}$ from Eq. (45) and (46).
6. If $\Delta p/\Delta p_{FLOOD}^{(1)} < 1$, expect mixed flow. Estimate: $\dot{V}_{NET} = \dot{V}_{NET}^{(1)}$ from Eqs. (52) and (54); $\dot{V}_{EX,MAX}$ and then $\dot{V}_{LOW} = \dot{V}_{LOW}^{(1)}$ from Eqs. (51), (53'), and (57); and $\dot{V}_{HIGH} = \dot{V}_{HIGH}^{(1)}$ from Eq. (58).

The algorithm is suitable for general use in zone-type compartment fire models.

APPLICATIONS OF VENTCL2: STEADY BURNING IN A CEILING-VENTED ROOM

Direct flow rate data to validate the **VENTCL2** model/algorithm are not available. However, there are data from full-scale ceiling-vented fire scenarios which can be used to validate the model indirectly. These scenarios are special cases of the important class of problem involving steady burning in a ceiling-vented room. In this section **VENTCL2** will first be used to obtain a general solution to this problem. Then, the solution will be compared to aspects of previously published data from two full-scale experimental studies involving the purely ceiling-vented fire scenario.

²The 2.5 exponent in Eq. (59) is different from that of Eq. (23) of [6] which seems to be printed incorrectly. Eq. (59) corresponds to the correlating function plotted in Figure 5 of [6].

The Problem

Consider a room with a fire, fully-enclosed except for a shallow circular ceiling vent. Refer to Figure 12. The outside air above the vent has ambient density, temperature, and oxygen mass concentration, T_{AMB} , ρ_{AMB} , and ψ_{AMB} , respectively. Assume steady conditions where the room environment immediately below the vent has density, temperature, and O_2 mass concentration ρ , $T > T_{AMB}$, and $\psi < \psi_{AMB}$, respectively. ψ_{LOW} , the O_2 mass concentration in the lower part of the room at the elevation of the fire, must exceed the minimum, extinction value, ψ_{EXT} , associated with the particular fuel. For example, for the combustion of CH_4 diffusion flames from round burners with diameters D in the range $0.50 \text{ m} \leq D \leq 0.089 \text{ m}$, ψ_{EXT} was measured by Morehart, Zukoski, and Kubota [14, 15] as ranging from 0.140 ($D = 0.50 \text{ m}$, $T = 1765 \text{ K}$) to 0.161 ($D = 0.089 \text{ m}$, $T = 1765 \text{ K}$). Note that under the conjectured steady state condition, the O_2 that supplies the lower part of the room and maintains it at a $\psi_{LOW} > \psi$ comes from the cool and relatively O_2 -rich ambient air that enters the ceiling vent and drops toward the floor of the room in a negatively buoyant plume.

In this section the **VENTCL2** algorithm will be used to estimate the exchange flow through the vent and the burning rate that can be supported by the net rate of oxygen inflow.

The Relationship Between Δp and T

Assume: the mass-flow-rate of fuel introduced by the fire is negligible compared to the mass-flow-rate of the exchange-flow; the environment inside and outside the room can be modeled as a perfect-gas approximation to air; and there is no mixing in the vent, i.e., all inflow is at the ambient condition and all outflow is at the upper room environment. Using the approximation of Eq. (3), it follows from Eq. (12) that

$$T/T_{AMB} \approx \rho_{AMB}/\rho = \rho_{TOP}/\rho_{BOT} > 1 \quad (61)$$

From Eqs. (4) and (61) it is evident that the present problem involves an unstable configuration, and that the **VENTCL2** flow algorithm is applicable.

Conservation of mass across the vent requires

$$\rho \dot{V}_{BOT} = \rho_{AMB} \dot{V}_{TOP} \quad (62)$$

where \dot{V}_{BOT} and \dot{V}_{TOP} are the volume flow rates from the bottom to the top of the vent and from the top to the bottom of the vent, respectively. Using Eq. (61), it follows from Eq. (62) that the high and low pressure sides of the vent are at the bottom and top, respectively, i.e., the problem involves a Problem 2 scenario in the mixed-flow regime.

$$\dot{V}_{HIGH} = \dot{V}_{BOT}; \dot{V}_{LOW} = \dot{V}_{TOP}; \rho_{HIGH} = \rho; \rho_{LOW} = \rho_{AMB} \quad (63)$$

According to the **VENTCL2** algorithm, replace ε by $\varepsilon' = -\varepsilon$ in the Problem 1 solution to obtain the desired Problem 2 solution. From the Eq. (13) and (16) definition of ε

$$\varepsilon' = -\varepsilon = -2(T^* - 1)/(T^* + 1) < 0; T^* = T/T_{AMB} = (2 - \varepsilon')/(2 + \varepsilon') \quad (64)$$

Also, define

$$\delta p^* = \Delta p / \Delta p_{\text{FLOOD}}^{(1)} \quad (65)$$

where, from Eq. (38')

$$\Delta p_{\text{FLOOD}}^{(1)} = 0.2427(4g\Delta\rho D)(1 + \varepsilon' / 2)\exp(1.1072\varepsilon') \quad (66)$$

VENTCL2 and Eq. (62) require the following functional dependence of δp^* on ε'

$$\phi(\delta p^*) = \lambda(\varepsilon') \quad (67)$$

where

$$\lambda(\varepsilon') = -2(0.282)\varepsilon' \exp(-0.5536\varepsilon') / (2 + \varepsilon') \quad (68)$$

$$\phi(\delta p^*) = \{M - [1 + (M^2 - 1)(1 - \delta p^*)]^{1/2}\} / \{(M - 1)[(1 + m_3/2)(1 - \delta p^*)^2 - (2 + m_3/2)(1 - \delta p^*)]^2\}$$

and where M and m_3 are given in Eqs. (54) and (57), respectively.

Using the numerical root-finder **RTSAFE** listed by Press [16], the solution of Eq. (67) for δp^* as a function of ε' or T/T_{AMB} was found for a wide range of $\varepsilon' < 0$ ($T > T_{\text{AMB}}$). This is plotted in Figure 13.

The Energy Release Rate of the Fire as a Function of T and Its Maximum Possible Value

The energy-release rate, \dot{Q} , of the fire is related to the net rate of oxygen inflow which is consumed entirely by the combustion.

Eqs. (51), (62), and (63) lead to

$$\begin{aligned} \text{net rate of O}_2 \text{ consumed} &= \psi_{\text{AMB}}\rho_{\text{AMB}}\dot{V}_{\text{LOW}} - \psi_{\text{HIGH}}\dot{V}_{\text{HIGH}} \\ &= 0.055D^{5/2}g^{1/2}|\varepsilon'|^{1/2}\psi_{\text{AMB}}\rho_{\text{AMB}}(1 - \psi/\psi_{\text{AMB}})\dot{V}_{\text{LOW}}/\dot{V}_{\text{EX,MAX}} \end{aligned} \quad (69)$$

where, $\dot{V}_{\text{LOW}}/\dot{V}_{\text{EX,MAX}} = \dot{V}_{\text{LOW}}^{(1)}/\dot{V}_{\text{EX,MAX}}^{(1)}$, a function of δp^* , is given in Eq. (53').

From Huggett [17]

$$C_{\text{O}_2} \equiv \dot{Q}/(\text{net rate of O}_2 \text{ consumed}) = 13.2(10^3)\text{kW}/(\text{kg}_{\text{O}_2}/\text{s}) \quad (70)$$

Using Eq. (69) in Eq. (70) and defining a dimensionless \dot{Q}

$$\dot{Q}^* \equiv \dot{Q} / [(1 - \psi / \psi_{AMB}) \rho_{AMB} \psi_{AMB} C_{O_2} A_V^{5/4} g^{1/2}] \quad (71)$$

leads to

$$\dot{Q}^* = 0.074 |\varepsilon'|^{1/2} \dot{V}_{LOW}^{(1)} / \dot{V}_{EX,MAX} \quad (72)$$

The previously determined δp^* vs ε solutions were used in Eqs. (72), (53'), and (64) to obtain \dot{Q}^* vs T/T_{AMB} and this is plotted in Figure 13. From this it is seen that \dot{Q}^* is predicted to rise rapidly from 0, at $T/T_{AMB} = 1$, to a maximum value, $\dot{Q}_{MAX}^* = 0.037$, at $T/T_{AMB} = 1.65$, and to monotonically decrease with further increases of T/T_{AMB} . Associated with \dot{Q}_{MAX}^* , let \dot{Q}_{MAX} be the maximum possible \dot{Q} for a given ψ . Taking $T_{AMB} = 300$ K, $\rho_{AMB} = 1.2$ kg/m³, $\psi_{AMB} = (0.23 \text{ kg O}_2)/\text{kg}$, and $g = 9.8$ m/s², Eqs. (70) and (71) lead to

$$\dot{Q}_{MAX} = 0.41(10^3) \{1 - \psi / [0.23(\text{kg O}_2)/\text{kg}]\} (A_V / \text{m}^2)^{5/4} \text{ kW} \quad (73)$$

The scenario, leading to the largest value of \dot{Q}_{MAX} , is one where ψ is negligible. This would likely be associated with $\psi_{LOW} \approx \psi_{EXT}$. Thus, from Eq. (73)

$$\dot{Q}_{MAX} < 0.41(10^3) (A_V / \text{m}^2)^{5/4} \text{ kW} = 0.41(10^3) \text{ kW}, 1.3 \text{ kW}, \text{ and } 0.23 \text{ kW for } A_V = \quad (74) \\ 1.0 \text{ m}^2, 1.0(10^{-2}) \text{ m}^2, \text{ and } 25.0(10^{-4}) \text{ m}^2, \text{ respectively}$$

The results of Figure 13 are now related to data acquired in "full-scale" experiments reported by Steward, Morrison, and Mehaffey [18] and Jansson, Onnermark, and Halvarsson [19]. In this it is assumed that the present circular-vent results can be used to provide estimates for the square- and rectangular-vented enclosures used in the experiments.

Experimental Validation of the Figure 13 Solution

Fire in Ceiling-Vented Ship Quarters. Steward, Morrison, and Mehaffey [18] report on a fire in a mock-up of a fully-furnished three-person ship accommodation quarter (3.84 m by 2.82 m by 2.38 m high), fully enclosed except for a single square vent, $A_V = 1.00$ m², in a corner of the ceiling, away from the furnishings. The fire involved an initial interval of intense burning which rapidly decayed to smoldering (10 minutes); an interval of smoldering (20 minutes), and a final interval of intense burning (30 minutes). The final interval involved a 19-20 minute sub-interval in which the heat release rate was relatively constant at $\dot{Q} = (0.25 \pm 0.05)10^3$ kW. It is reasonable to expect that the latter sub-interval was a time of steady state during which the present example analysis of ventilation conditions is relevant. Indeed, the measured burn rate does satisfy the criterion of Eq. (74), i.e., $\dot{Q} = (0.25 \pm 0.05)10^3$ kW $< \dot{Q}_{MAX} = 0.41(10^3)$ kW. Also, $\psi = 0.09$ (kg O₂)/kg was estimated from Eq. (73). There is no reported measured value to validate the latter result. However, the result is plausible since, as required, it is clearly less than the likely value of $\psi_{LOW} \approx \psi_{EXT}$.

Note that because of the original assumption of no mixing in the vent, the $\dot{Q}_{MAX} = 0.41(10^3)$ kW and $\psi = 0.09$ (kg O₂)/kg estimates must be regarded as upper and lower bounds, respectively, to the actual expected values. Thus, the actual rate of O₂ inflow would be less than $\psi_{AMB}\rho_{AMB}\dot{V}_{TOP}$ and the rate of O₂ outflow would be greater than $\psi\rho\dot{V}_{BOT}$.

Wood Fires in a Ceiling-Vented 27 m³ Cubic Enclosure. Jansson, Onnermark, and Halvarsson [19] report on 5 experiments involving wood fires located at the center of the floor of a cubic room (6.00 m by 6.00 m by 6.00 m), fully enclosed except for a single, centrally-located, ceiling vent. Three different vents were used: $A_v = 4.00$ m² (square), 2.00 m² (1.00 m by 2.00 m), and 1.00 m² (square). The burn times were 30 min. Measured and reported variables included: dM/dt , where M is the mass of the fuel; $T_{UP,AVE}$, the average of the upper-enclosure temperatures; and c_{LOW,O_2} and c_{LOW,CO_2} , the molal fractions of O₂ and CO₂ in the lower part of the enclosure, 1 m from the floor and 1 m from the combustion zone. The data were studied to identify intervals that could be reasonably construed to represent quasi-steady-state conditions for which the present example calculation would be relevant. The selected criterion for this was that all measured variables reported by Jansson, Onnermark, and Halvarsson [19] were relatively constant over an interval of at least 5 min.

The "best" steady state interval was found and analyzed for experiments 2, 3, and 4. No steady state intervals were identified in experiments 1 and 5.

For the experiments the heat of combustion of the wood fuel was taken from Drysdale [20] to be 19.5 kJ/g and it was assumed that the smoke yield was negligible. Then, for the intervals of steady state burning the Figure 13 results and Eqs. (70) and (71) were used to estimate ψ from \dot{Q}_{MEAS} (the measured values of \dot{Q} as deduced from the measured values of dM/dt) and from T (estimated to be identical to $T_{UP,AVE}$).

The results of the analyses are summarized in Table 4. In the table, ψ_{LOW} was estimated from c_{LOW,O_2} according to $\psi_{LOW} \approx 0.23(c_{LOW,O_2}/0.21)$.

Note that the low ψ_{LOW} values of Experiments 2 and 3, approximately 0.15, indicate that the fire in both cases was close to extinction. The measured values of c_{LOW,O_2} in these two cases were 0.137 ± 0.004 and 0.141 ± 0.002 for experiments 2 and 3, respectively; these are the lowest O₂ concentrations measured throughout the entire test series of Jansson, Onnermark, and Halvarsson [19].

As in the analysis of [19], there are no reported measured values of ψ to directly confirm the calculated results of Table 4. However, once again the calculated results are plausible, since, as required, they are always less than ψ_{LOW} . As with the previous example, the results are also consistent with the original assumption of no mixing in the vent in that it is reasonable to anticipate that actual values of ψ , expected to be greater than the presently predicted values of Table 4, would, as required, also be less than the corresponding values of ψ_{LOW} . Thus, in experiment 2, for example, it is expected that the experimental value of ψ was somewhat greater than 0.08, while still being less than $\psi_{LOW} \approx 0.15$.

ACKNOWLEDGMENTS

Much of the work presented here was done while the author was a guest of the Fire Research Institute of Japan. The author acknowledges gratefully the gracious hospitality and very useful discussions with the staff of that institution during that visit, and especially with Dr. Tokiyoshi Yamada.

NOMENCLATURE

A_V	vent area
C_D ; $C_D^{(N)}$; $C_{D,HS}$; $C_{D,\infty}$; $C_{D,FLOOD}$	vent flow coefficient, Eq. (5); C_D for Problem N; C_D of [10]; C_D at large Reynolds number; C_D at onset of flooding
C_{O_2}	Eq. (70)
C_p	specific heat at constant pressure
c_{LOW,O_2} ; c_{LOW,CO_2}	molal fractions of O_2 , CO_2 in lower part of enclosure
D	characteristic span of vent opening
Fr_{HS}	Eq. (10), Froude number of [10]
$\bar{Fr}_{HIGH}^{(N)}$; $\bar{Fr}_{LOW}^{(N)}$; $\bar{Fr}_{HIGH,FLOOD}^{(N)}$	Froude numbers for Problem N, Eqs. (22) and (23); $\bar{Fr}_{HIGH}^{(N)}$ at onset of flooding
Gr_{HS} ; \bar{Gr}	Eq. (10), Grashof number of [10]; Grashof number, Eq. (17)
g	acceleration of gravity
k	thermal conductivity
L	depth of vent
M	Eqs. (52) and (54), also, mass of fuel [19]
m_N	Eqs. (50) for $N = 1$; (53) and (56) for $N = 2$; (53') and (55) for $N = 3$; (59) for $N = 4$
p ; $p^{(N)}$; $p^{*(N)}$; p_{HIGH} ; p_{LOW}	pressure; p for Problem N; dimensionless $p^{(N)}$, Eq. (15); far-field p on high-, low-pressure side of vent, near the vent elevation
\bar{p}	$(p_{HIGH} + p_{LOW})/2$
\bar{Pr}	Prandtl number, Eq. (17)
Q ; Q_{MEAS} ; Q_{MAX}	burning rate; Q measured in [19]; maximum of Q
Q^*	dimensionless Q , Eq. (71)
R	gas constant
T ; $T^{(N)}$; $T^{*(N)}$; T_{TOP} ; T_{BOT} ; T_{AMB} ; T ; $T_{UP,AVE}$	absolute temperature; T for problem N; dimensionless $T^{(N)}$, Eq. (15); far field T in top, bottom space; T of ambient; T/T_{AMB} ; average of upper-enclosure T measured in [19]

\bar{T}	$(T_{TOP} + T_{BOT})/2$
$U_i^{(N)}, U_i^{*(N)}, U_3^{(N)}$	velocity for Problem N; dimensionless $U_i^{(N)}$, Eq. (15); average $U_3^{(N)}$ at vent, Eq. (21)
$\dot{V}_{EX}, \dot{V}_{EX,MAX}$	exchange flow rate, \dot{V}_{LOW} ; maximum \dot{V}_{EX} , i.e., at $\Delta p = 0$
\dot{V}_{FLOOD}	\dot{V}_{HIGH} at onset of flooding
$\dot{V}_{HIGH}, \dot{V}_{HIGH,ST}$	volumetric flow rate from high- to low-pressure side of vent; \dot{V}_{HIGH} for standard flow model;
$\dot{V}_{LOW}, \dot{V}_{LOW,ST}$	volumetric flow rate from low- to high-pressure side of vent; \dot{V}_{LOW} for standard flow model
$\dot{V}_{HIGH}^{(N)}, \dot{V}_{HIGH,FLOOD}^{(N)}$	\dot{V}_{HIGH} for Problem N, Eq. (21); $\dot{V}_{HIGH}^{(N)}$ at onset of flooding
$\dot{V}_{NET}, \dot{V}_{NET}^{(N)}$	$\dot{V}_{HIGH} - \dot{V}_{LOW}$; \dot{V}_{NET} for Problem N
$X_i^{(N)}, X_i^{*(N)}$	cartesian coordinates for Problem N, Figure 2; dimensionless X_i , Eq. (15)
$\Delta p, \Delta p_{FLOOD}, \Delta p_{FLOOD}^{(N)}$	$p_{HIGH} - p_{LOW}$; Δp at onset of flooding; Δp_{FLOOD} for Problem N
ΔT	$T_{BOT} - T_{TOP}$
$\Delta \rho$	$\rho_{TOP} - \rho_{BOT}$
δp^*	$\Delta p / \Delta p_{FLOOD}^{(1)}$
$\varepsilon; \varepsilon'$	dimensionless $\Delta \rho, \Delta T$, Eq. (16); Eq. (64)
λ	Eq. (68)
$\mu; \bar{\mu}$	dynamic viscosity; Eq. (11)
ν	kinematic viscosity, Table 1
$\Pi; \Pi_{FLOOD}^{(N)}$	dimensionless Δp , Eq. (17); dimensionless $\Delta p_{FLOOD}^{(N)}$, Eq. (28)
$\rho; \rho^{(N)}, \rho^{*(N)}, \rho_{TOP}, \rho_{BOT}$	density; ρ for Problem N; dimensionless $\rho^{(N)}$, Eq. (15); far-field ρ in top, bottom space
$\bar{\rho}$	$(\rho_{TOP} + \rho_{BOT})/2$
$\sigma_{HIGH}^{(N)}, \sigma_{LOW}^{(N)}$	Eq. (20)
σ_1, σ_2	Eqs. (44) and (45)
ϕ	Eqs. (67) and (68)
$\psi, \psi_{AMB}, \psi_{LOW}$	mass concentration of O_2 in enclosure, of ambient, in lower part of enclosure

REFERENCES

- [1] Emmons, H., SFPE Handbook of Fire Protection Engineering, Sect. 1/Chapter 8, SFPE, Boston, pp. 130-138, 1988.
- [2] Cooper, L.Y., Calculation of the Flow Through a Horizontal Ceiling/Floor Vent, NISTIR 89-4052, National Institute of Standards and Technology, Gaithersburg MD, 1989.
- [3] Peacock, R.D. *et al*, CFAST, the Consolidated Model of Fire Growth and Smoke Transport, NIST TN 1299, National Institute of Standards and Technology, Gaithersburg MD, 1993.
- [4] Taylor, G. I., The Instability of Liquid Surfaces When Accelerated in a Direction Perpendicular to Their Planes, *Proc. Roy. Soc., A*, 201, pp. 192-196, 1950.
- [5] Epstein, M., Buoyancy-Driven Exchange Flow Through Small Openings in Horizontal Partitions, *J. Heat Transfer*, 110, pp. 885-893, 1988.
- [6] Brown, W.G., Natural Convection Through Rectangular Openings in Partitions - 2. Horizontal Partitions, *Int. J. Heat Mass Transfer*, 5, pp. 869-878, 1962.
- [7] Epstein, M. and Kenton, M.A., Combined Natural Convection and Forced Flow Through Small Openings in a Horizontal Partition With Special Reference to Flows in Multicompartent Enclosures, *J. Heat Transfer*, 111, pp. 980-987, 1989.
- [8] Tan, Q. and Jaluria, J., Flow Through Horizontal Vents as Related to Compartment Fire Environments, Rutgers University Report to NIST, National Institute of Technology, Gaithersburg MD, December 1991.
- [9] Perry, J.A., Critical Flow Through Sharp-Edged Orifices, *Trans. American Soc. Mech. Eng.*, 71, pp. 757-764, 1949.
- [10] Heskestad, G. and Spaulding, R.D., Inflow of Air Required at Wall and Ceiling Apertures to Prevent Escape of Fire Smoke, *Proceedings of the 3rd International Symposium on Fire Safety Science*, Elsevier, pp. 919-928, 1991.
- [11] Cooper, L.Y., An Algorithm and Associated Computer Subroutine for Calculating Flow Through a Horizontal Ceiling/Floor Vent in a Zone-Type Compartment Fire Model, NISTIR 4402, National Institute of Technology, Gaithersburg MD, 1990.
- [12] Cooper, L.Y., Combined Buoyancy- and Pressure-Driven Flow Through a Horizontal Vent: Theoretical Considerations, NISTIR 5252, National Institute of Standards and Technology, Gaithersburg MD, September 1993.
- [13] Hilsenrath, J., *et al*, *Tables of Thermal Properties of Gases*, NBS circular 564, National Institute of Standards and Technology (presently the National Institute of Standards and Technology), Gaithersburg MD, Nov. 1955.
- [14] Morehart, J.H., Zukoski, E.E., and Kubota, T., Characteristics of Large Diffusion Flames Burning in a Vitiated Atmosphere, Fire Safety Science - Proceedings of 3rd International Symposium, Eds. Cox, G., and Langford, B., Elsevier, pp. 575-583, 1991.

- [15] Morehart, J.H. Zukoski, E.E., Kubota, T., Species Produced in Fires Burning in Two-Layered and Homogeneous Vitiated Environments, California Institute of Technology October 1988 Quarterly Report to National Institute of Standards and Technology, Gaithersburg, August 1990.
- [16] Press, W.H. *et al*, Numerical Recipes, Cambridge, p.258, 1986.
- [17] Huggett, C., *Fire and Materials*, 4, pp. 61-65, 1980.
- [18] Steward, F.R., Morrison, L., and Mehaffey, J., Full Scale Fire Tests for Ship Accomodation Quarters, *Fire Technology*, pp. 31-47, Vol. 28, No. 7, Feb. 1992.
- [19] Jansson, R., Onnermark, B., Halvarsson, K., Fire in a Roof-Ventilated Room, FOA Report C 20606-D6, National Defence Research Institute, Stockholm, Sweden, March 1986.
- [20] Drysdale, D., An Introduction to Fire Dynamics, Wiley, p. 179, 1985.

Test ^{1}	ε	$\bar{Fr}_{HIGH}^{(1)}$	Π	$C_D^{(1)}$	$\bar{Gr}^{(6)}$	$\bar{Fr}_{HIGH}^{(1)}/\bar{Fr}_{HIGH,FLOOD}^{(1)}$	$C_D^{(1)}/C_{D,\infty}^{(5)}$	$\Pi/\Pi_{FLOOD}^{(1)}$
54 ^{2}	0.521	0.216	0.601	0.156	2.99(10 ⁷)	0.924	0.261	1.10
55 ^{2}	0.559	0.243	0.532	0.188	3.49(10 ⁷)	1.02	0.314	0.923
56 ^{2}	0.282	0.186	0.467	0.146	4.64(10 ⁷)	0.910	0.243	1.24
59 ^{2}	0.373	0.227	0.392	0.198	4.74(10 ⁷)	1.05	0.329	0.901
60 ^{2}	0.474	0.238	0.456	0.196	4.06(10 ⁷)	1.04	0.326	0.900
61 ^{2}	0.260	0.248	0.382	0.214	4.66(10 ⁷)	1.23	0.356	1.04
53 ^{3}	0.521	0.257	0.657	0.178	2.99(10 ⁷)	1.10	0.296	1.21
53 ^{3,4}	0.521	0.474	0.708	0.316	2.99(10 ⁷)	2.03	0.527	1.30
53 ^{3,4}	0.521	0.661	0.848	0.403	2.99(10 ⁷)	2.83	0.671	1.56
53 ^{3,4}	0.521	0.814	0.111	0.434	2.99(10 ⁷)	3.48	0.723	2.04
54 ^{4}	0.521	0.461	0.631	0.326	2.99(10 ⁷)	1.97	0.543	1.16
55 ^{4}	0.559	0.262	0.455	0.219	3.49(10 ⁷)	1.10	0.366	0.790
56 ^{4}	0.282	0.342	0.603	0.235	4.64(10 ⁷)	1.67	0.392	1.59

{1} See TABLES III and VI of Heskestad and Spaulding [10].

{2} Identified in Heskestad and Spaulding [10] as the flooding condition, i.e., the $\bar{Fr}_{HIGH}^{(1)}$, Π , and $C_D^{(1)}$ values for this datum point are $\bar{Fr}_{HIGH,FLOOD}^{(1)}$, $\Pi_{FLOOD}^{(1)}$, and $C_{D,FLOOD}^{(1)}$, respectively.

{3} Same fuel and fuel flow rate as Test Condition 54.

{4} T_{TOP} and T_{BOT} are not presented by Heskestad and Spaulding [10]; it is assumed here that the values of these were the same as the values measured in the same test, i.e., the same fuel and fuel flow rate, but at flooding conditions.

{5} $C_{D,\infty}$ is taken to be 0.60; $\bar{Fr}_{HIGH,FLOOD}^{(1)} = \bar{Fr}_{HIGH,FLOOD}^{(1)}(\varepsilon, \bar{Gr} \rightarrow \infty)$ and $\Pi_{FLOOD}^{(1)} = \Pi_{FLOOD}^{(1)}(\varepsilon, \bar{Gr} \rightarrow \infty)$ are calculated from Eqs. (37) - (39).

{6} In calculating \bar{Gr} from Eq. (17), the kinematic viscosity, $\nu(\bar{T}) = \mu(\bar{T})/\bar{\rho}$, determined from Hilsenrath [13]

$$\nu(\bar{T}) = [0.04128(\bar{T}/K)^{5/2}(10^{-7})/(\bar{T}/K + 110.4)]m^2/s$$

Table 1. Results derived from the configuration-1 experimental data of Heskestad and Spaulding [10] for flow through a $D = 0.153m$, $L/D = 0.011$ circular vent, and from Eqs. (37) and (38') for $\bar{Fr}_{HIGH,FLOOD}^{(1)}$ and $\Pi_{FLOOD}^{(1)}$.

Reference Number	ε	Configuration Number	$\bar{F}_{r,HIGH,FLOOD}^{(1)}$	$\bar{G}r$	$C_{D,FLOOD}^{(1)}$	$\Pi_{FLOOD}^{(1)}$
[10]	0.521	1	0.216	$2.99(10^7)$	0.156	0.601
[10]	0.559	1	0.243	$3.49(10^7)$	0.188	0.532
[10]	0.282	1	0.186	$4.64(10^7)$	0.146	0.467
[10]	0.373	1	0.227	$4.74(10^7)$	0.198	0.392
[10]	0.474	1	0.238	$4.06(10^7)$	0.196	0.456
[10]	0.260	1	0.248	$4.66(10^7)$	0.214	0.382
[7]	0.1426	1	0.1917	$5.31(10^7)$	{1}	{1}
[7]	0.1410	1	0.1755	$5.25(10^7)$	{1}	{1}
[7]	0.1378	2	0.1632	$5.13(10^7)$	{1}	{1}
[7]	0.1487	1	0.2057	$5.54(10^7)$	{1}	{1}
[7]	0.1339	2	0.1783	$4.98(10^7)$	{1}	{1}
[7]	0.1456	1	0.1826	$2.91(10^8)$	{1}	{1}
[7]	0.1329	1	0.1709	$2.66(10^8)$	{1}	{1}
[7]	0.1417	1	0.1618	$2.84(10^8)$	{1}	{1}
[8]	0.0469	2	0.2534	$4.28(10^6)$	0.0966	1.638
[8]	0.0658	2	0.4383	$6.00(10^6)$	0.194	1.191
[8]	0.0898	2	0.3463	$8.20(10^6)$	0.168	0.970
[8]	0.1208	2	0.4132	$1.10(10^7)$	0.218	0.793
[8]	0.1550	2	0.3877	$1.41(10^7)$	0.220	0.659

{1} This value is not available since Δp was not measured

Table 2. Small-L/D data on flooding conditions from Epstein and Kenton [7], Tan and Jaluria [8], and Heskestad and Spaulding [10].

Vent Type	D	L/D	$\dot{V}_{NET}^{(1)}/\dot{V}_{HIGH,FLOOD}^{(1)}$	$\dot{V}_{LOW}^{(1)}/\dot{V}_{EX,MAX}^{(1)}$
disk	0.02540	0.01902	0.5331	0.1743
disk	0.02540	0.01902	0.4329	0.2729
disk	0.02540	0.01902	0.1068	0.7588
disk	0.02540	0.1130	0.2996	0.5270
tube	0.02540	0.5000	0.09279	0.6917
tube	0.02540	0.5000	0.2936	0.3108
tube	0.02540	1.000	0.1957	0.5045
tube	0.02540	1.000	0.5661	0.1180
tube	0.02540	1.000	0.4541	0.1504
tube	0.02540	1.000	0.2113	0.4741
tube	0.02540	2.000	0.4659	0.1728
tube	0.02540	2.000	0.5088	0.1362
tube	0.02540	2.000	0.2663	0.2920
tube	0.02540	5.000	0.1992	0.5693
tube	0.02540	5.000	0.4456	0.2213
tube	0.02540	5.000	0.2442	0.4428
tube	0.04450	0.3910	0.09980	0.7067
tube	0.04450	0.3910	0.4983	0.1472
tube	0.04450	0.3910	0.3049	0.3706
tube	0.04450	0.3910	0.2190	0.4821

{1} $\dot{V}_{NET}^{(1)}$ and $\dot{V}_{LOW}^{(1)}$ are from Table 2 of Epstein and Kenton [7]; $\dot{V}_{EX,MAX}$ and $\dot{V}_{HIGH,FLOOD}^{(1)}$ are from Eqs. (21) and (22) of Epstein and Kenton [7], respectively.

Table 3. $\dot{V}_{NET}^{(1)}/\dot{V}_{HIGH,FLOOD}^{(1)}$ vs $\dot{V}_{LOW}^{(1)}/\dot{V}_{EX,MAX}$ results from Epstein and Kenton [7] in the mixed flow regime for flow through circular vents or disks and tubes.

Exp't. no., interval, initial mass	A_V [m ²]	$T_{UP,AVE}$ [K]	Q_{MEAS} [kW]	ψ [(kg O ₂)/kg]	ψ_{Low} [(kg O ₂)/kg]
2, 15-20 min, 100 kg	2	440 +/- 6	620. +/- 60	0.08	0.15 +/- 0.004
3, 15-20 min, 100 kg	1	386 +/- 1	250. +/- 10	0.07	0.15 +/- 0.002
4, 5-10 min, 25 kg	4	373 +/- 5	550. +/- 100	0.16	0.21 +/- 0.003

Table 4. Data on ceiling-vented wood fire scenarios of Jansson, Onnermark, and Halvarsson [19] and application of Figure 13 and Eqs. (70) and (71).

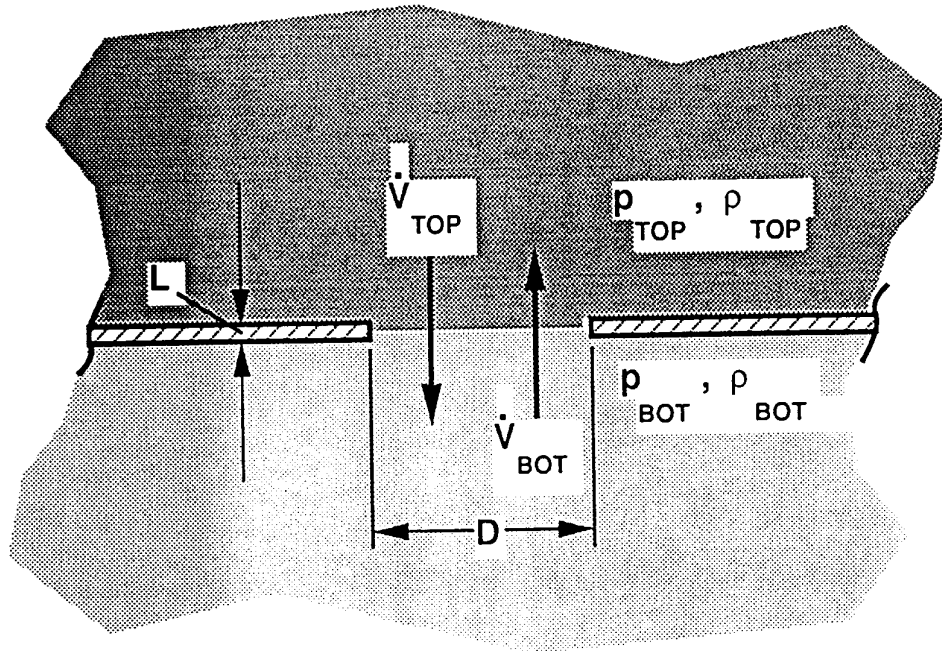
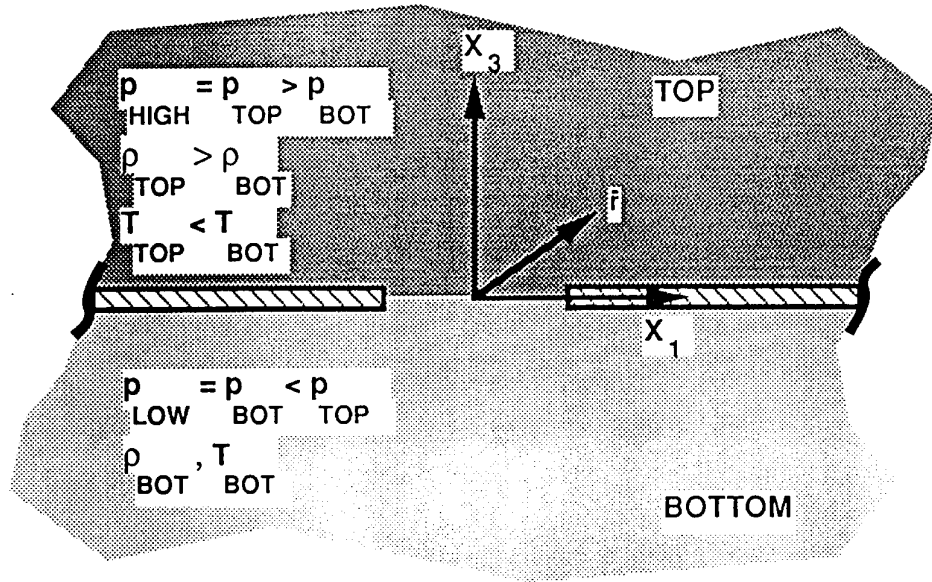
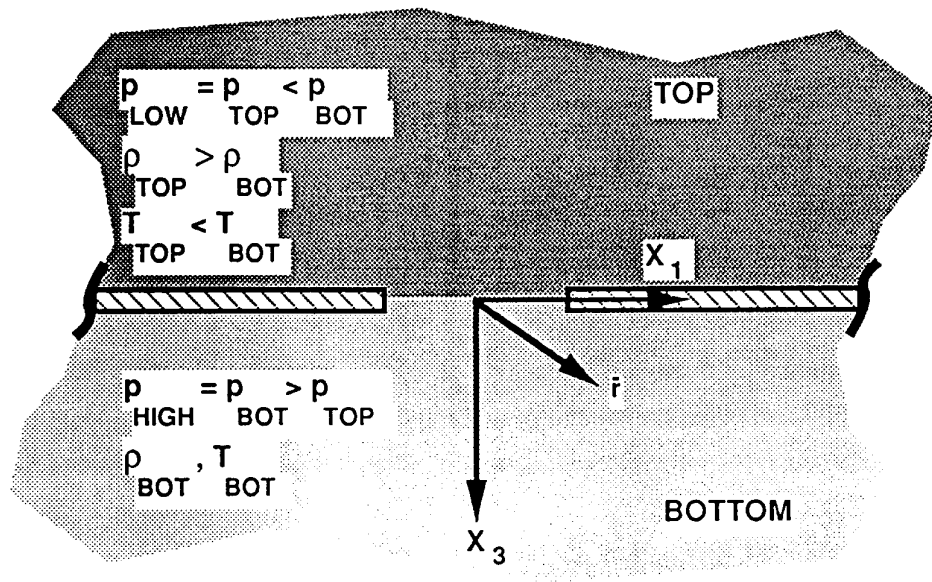


Figure 1. The basic horizontal-vent configuration.

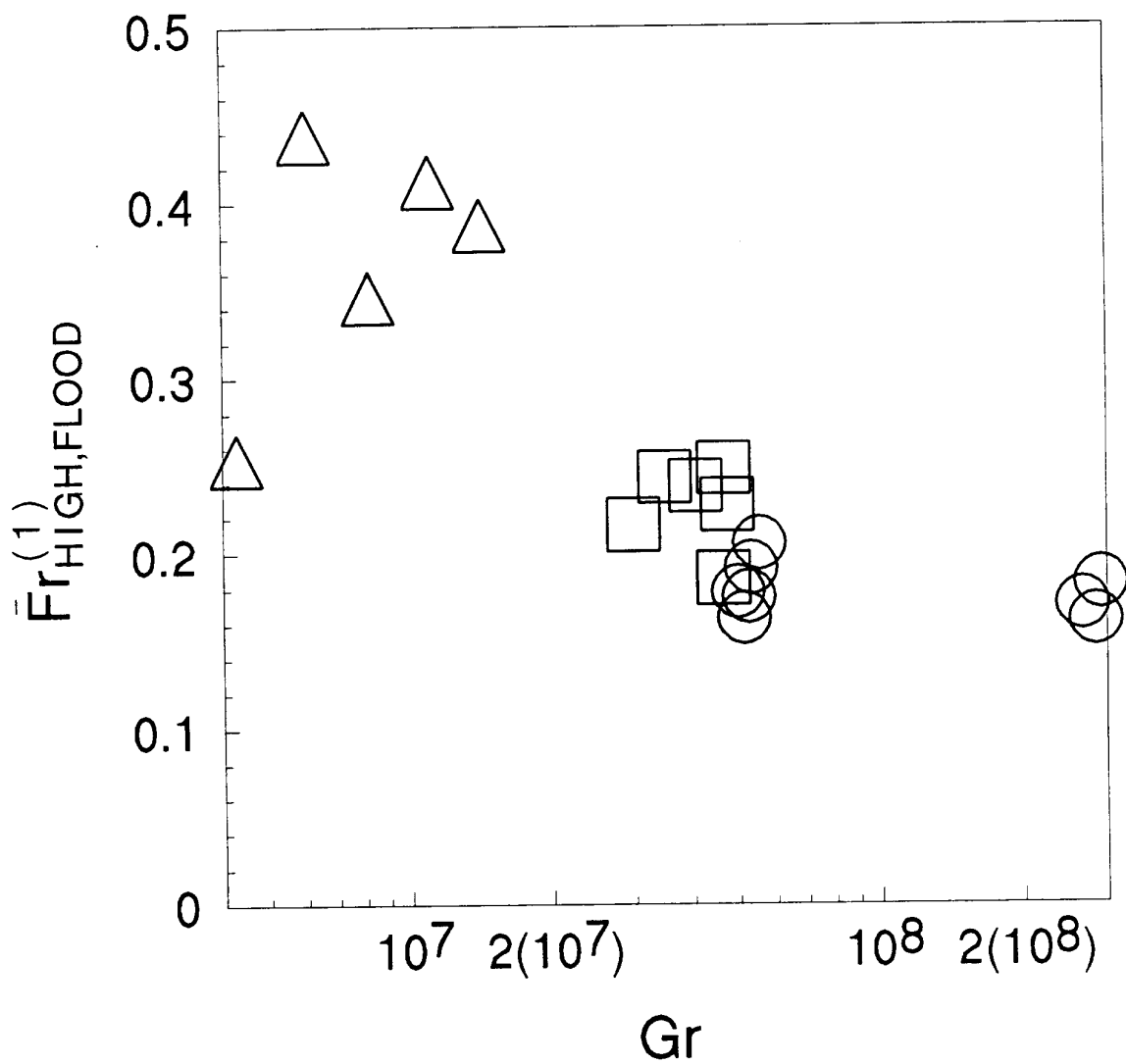


(a)



(b)

Figure 2. (a) Configuration 1 and (b) Configuration 2 illustrating conditions associated with boundary value problems 1 and 2, respectively.



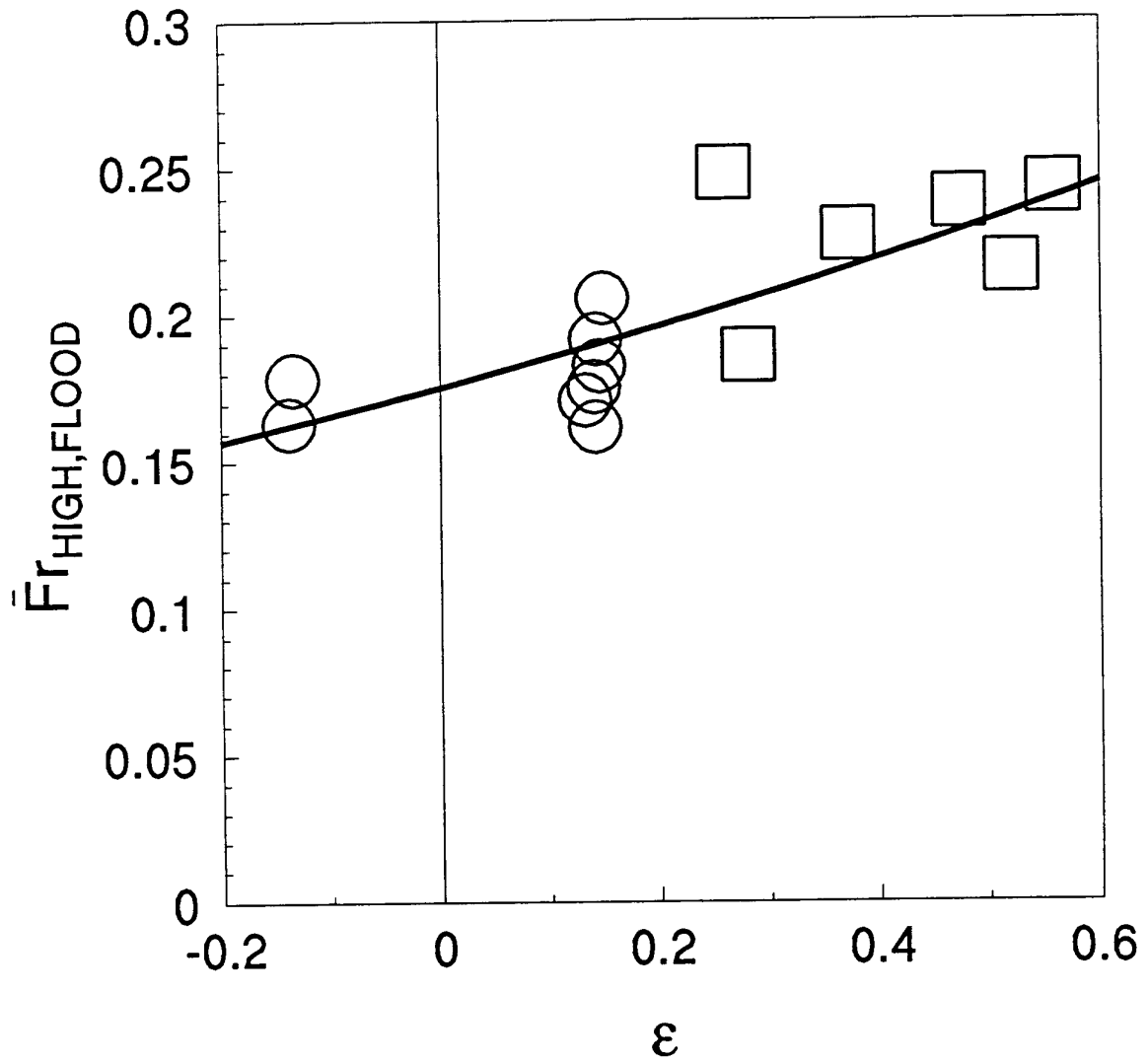


Figure 4. Plot of $\bar{Fr}_{HIGH,FLOOD}^{(1)}(\epsilon)$: data of Table 2 (O - Ref. [6], □ - Ref. [9]); —, least-squares curve fit of Eq. (37).

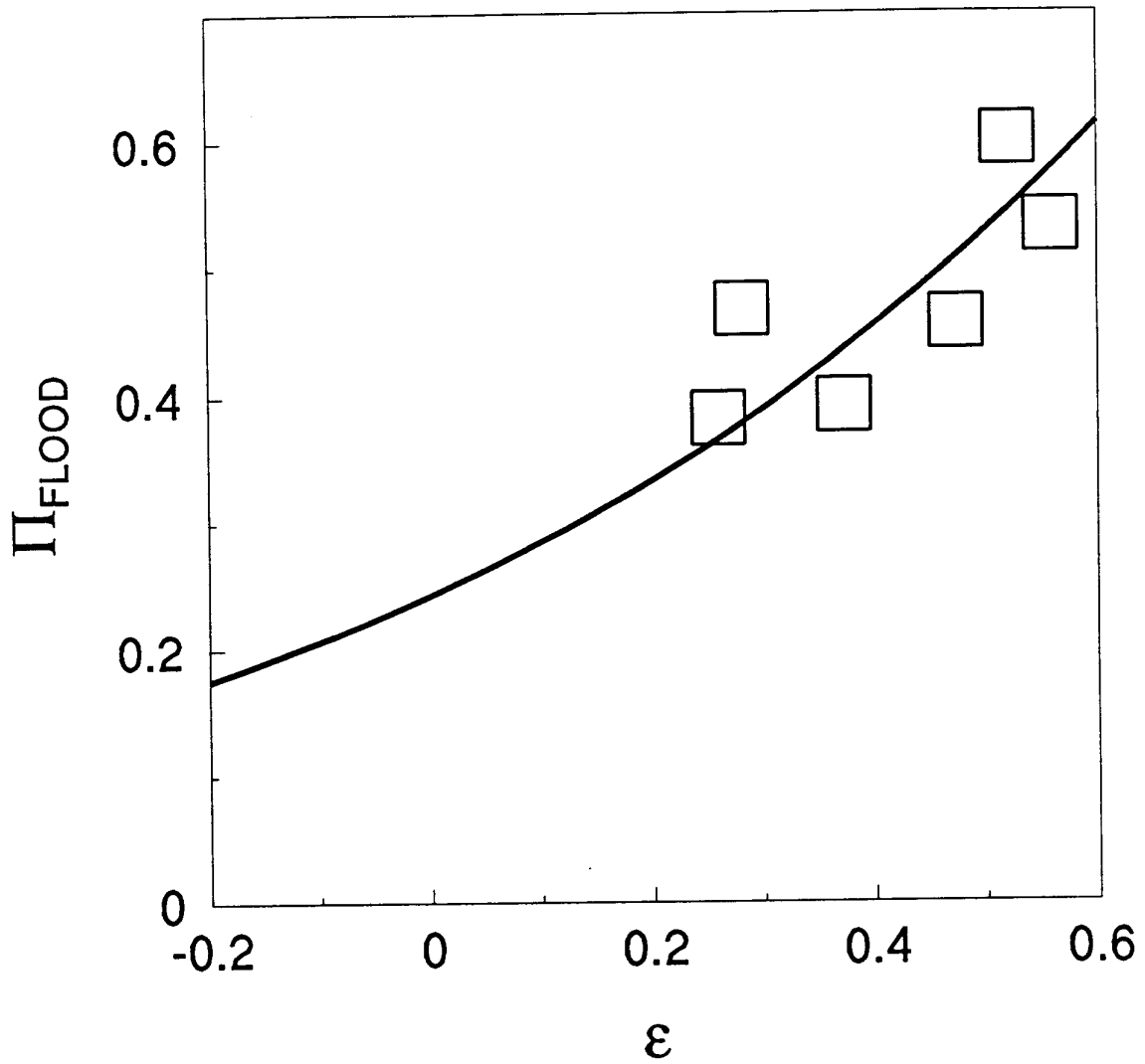


Figure 5. Plot of the $\Pi_{\text{FLOOD}}^{(1)}(\epsilon)$: \square - Ref. [9] data of Table 2; —, least-squares curve fit of Eq. (38').

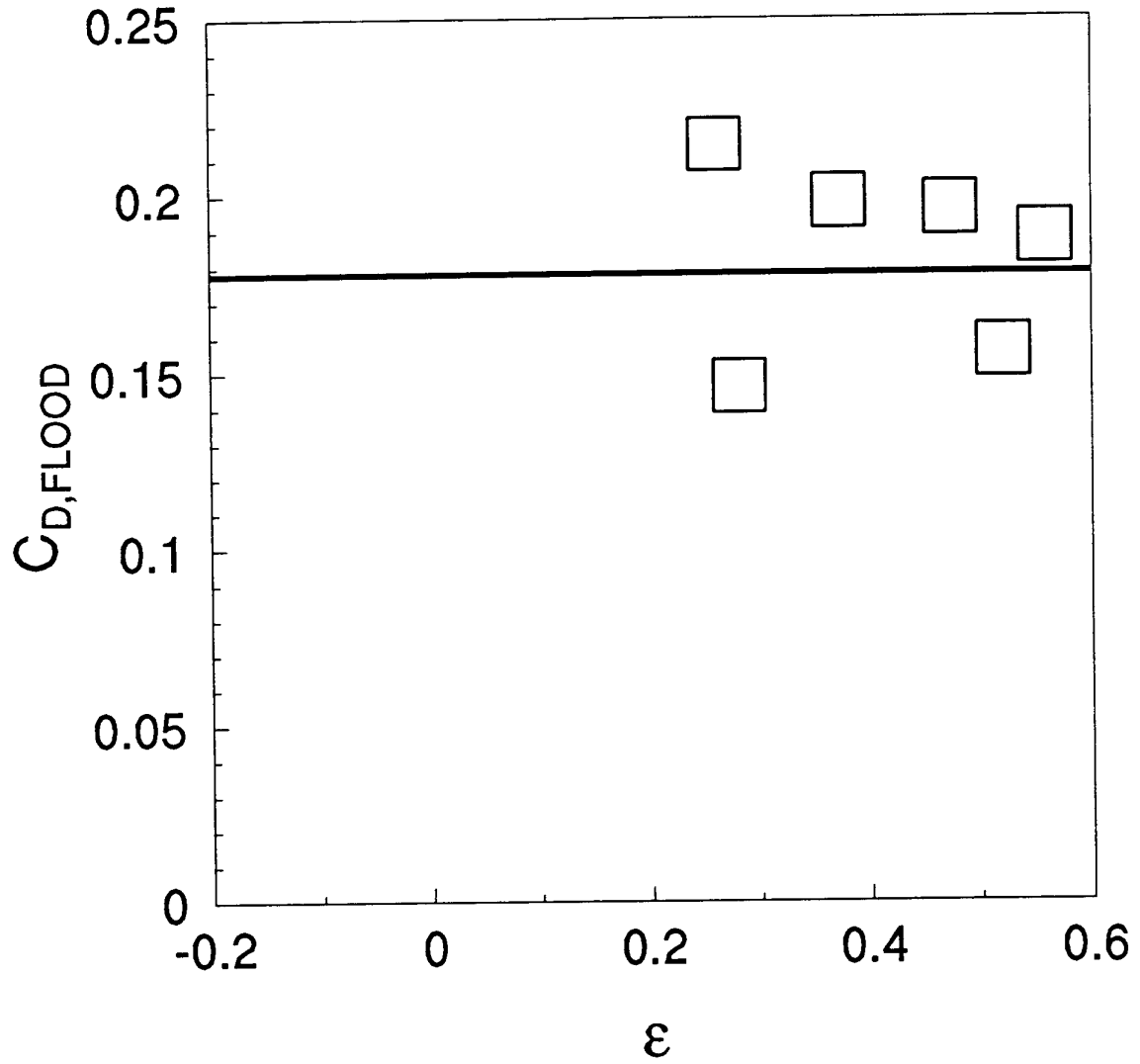


Figure 6. Plot of $C_{D,FLOOD}^{(1)}(\epsilon)$: \square - Ref. [9] data of Table 2; —, curve fit of Eq. (39).

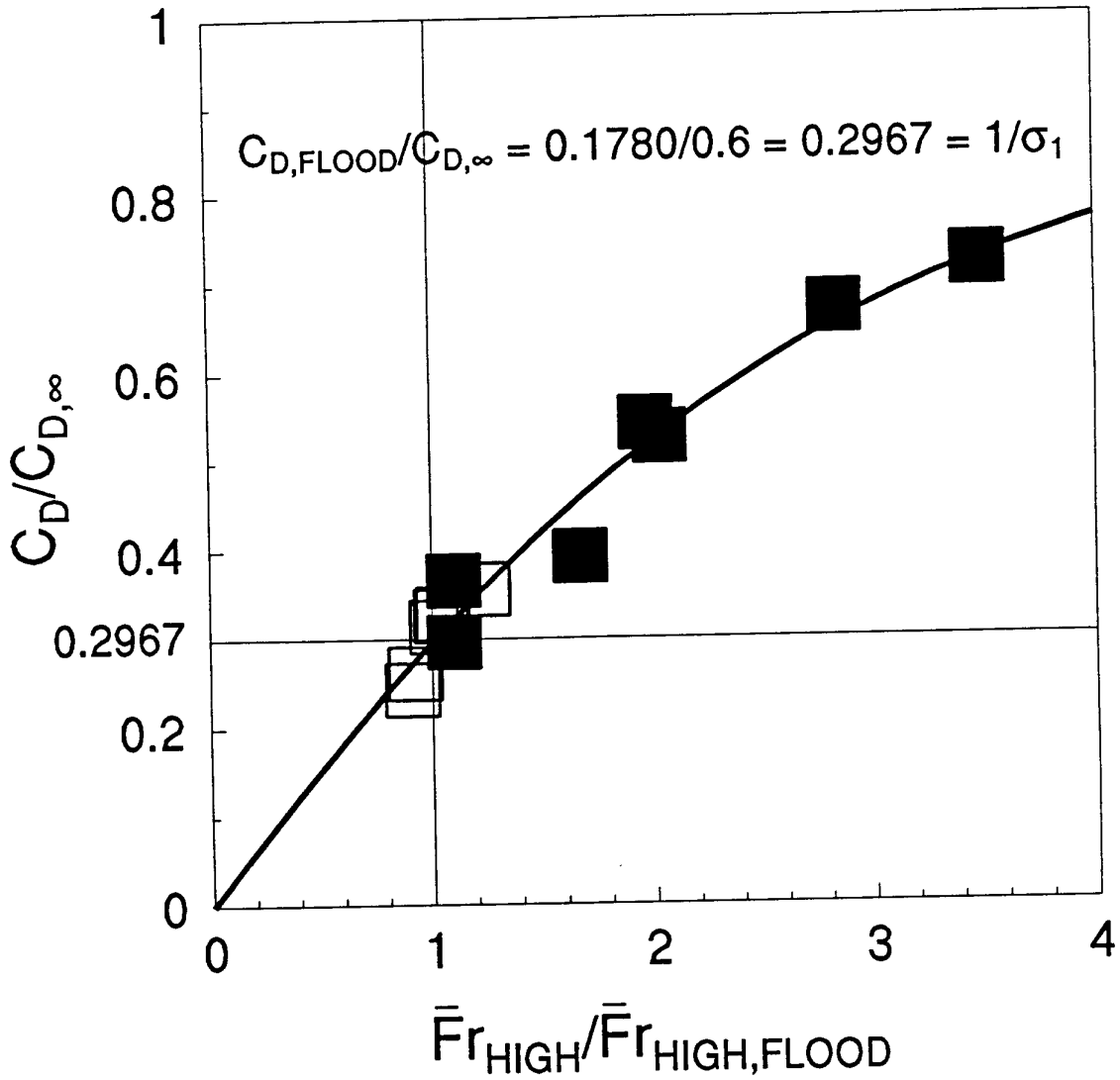


Figure 7. Plot of $C_D^{(1)}/C_{D,\infty}$ vs $\bar{Fr}_{HIGH}^{(1)}/\bar{Fr}_{HIGH,FLOOD}^{(1)}$: —, Eq. (44) and (45); ■, non-flooding data of Table 1; □, flooding data of Table 1.

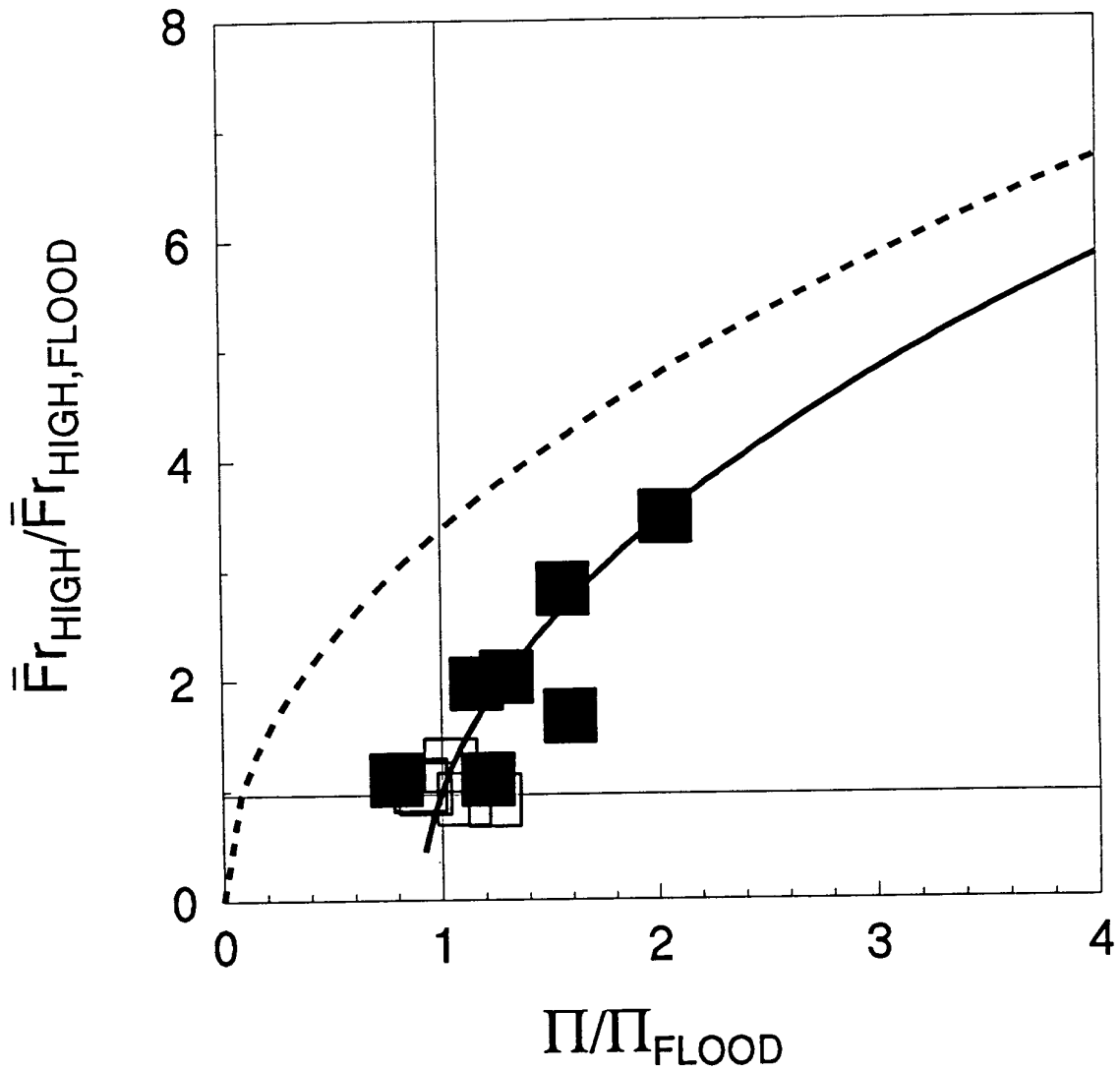


Figure 8.

Plot of $\bar{V}_{HIGH}/\bar{V}_{HIGH,FLOOD} = Fr_{HIGH}^{(1)}/Fr_{HIGH,FLOOD}^{(1)}$ vs $\Delta p/\Delta p_{FLOOD}^{(1)} = \Pi/\Pi_{FLOOD}^{(1)}$: —, model equation for the uni-directional flow regime, Eqs. (45) and (46); ---, Bernoulli flow limit of Eq. (48); ■, non-flooding data of Table 1; □, flooding data of Table 1.

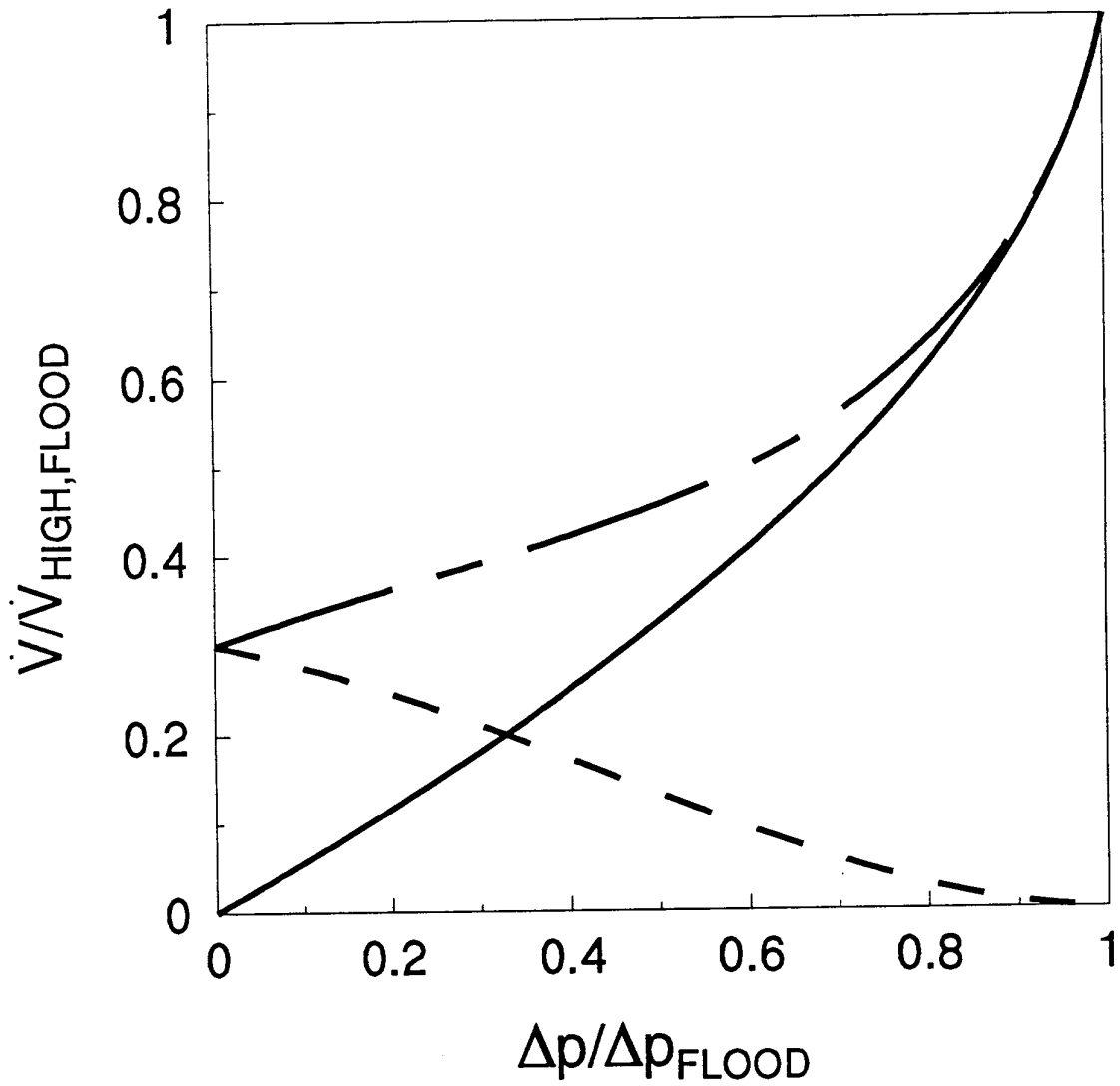


Figure 9. Sketch of $V_{\text{HIGH}}^{(1)} / V_{\text{HIGH,FLOOD}}^{(1)}$, $V_{\text{LOW}}^{(1)} / V_{\text{HIGH,FLOOD}}^{(1)}$, and $V_{\text{NET}}^{(1)} / V_{\text{HIGH,FLOOD}}^{(1)}$, as functions of $\Delta p / \Delta p_{\text{FLOOD}}$ in the mixed flow regime.

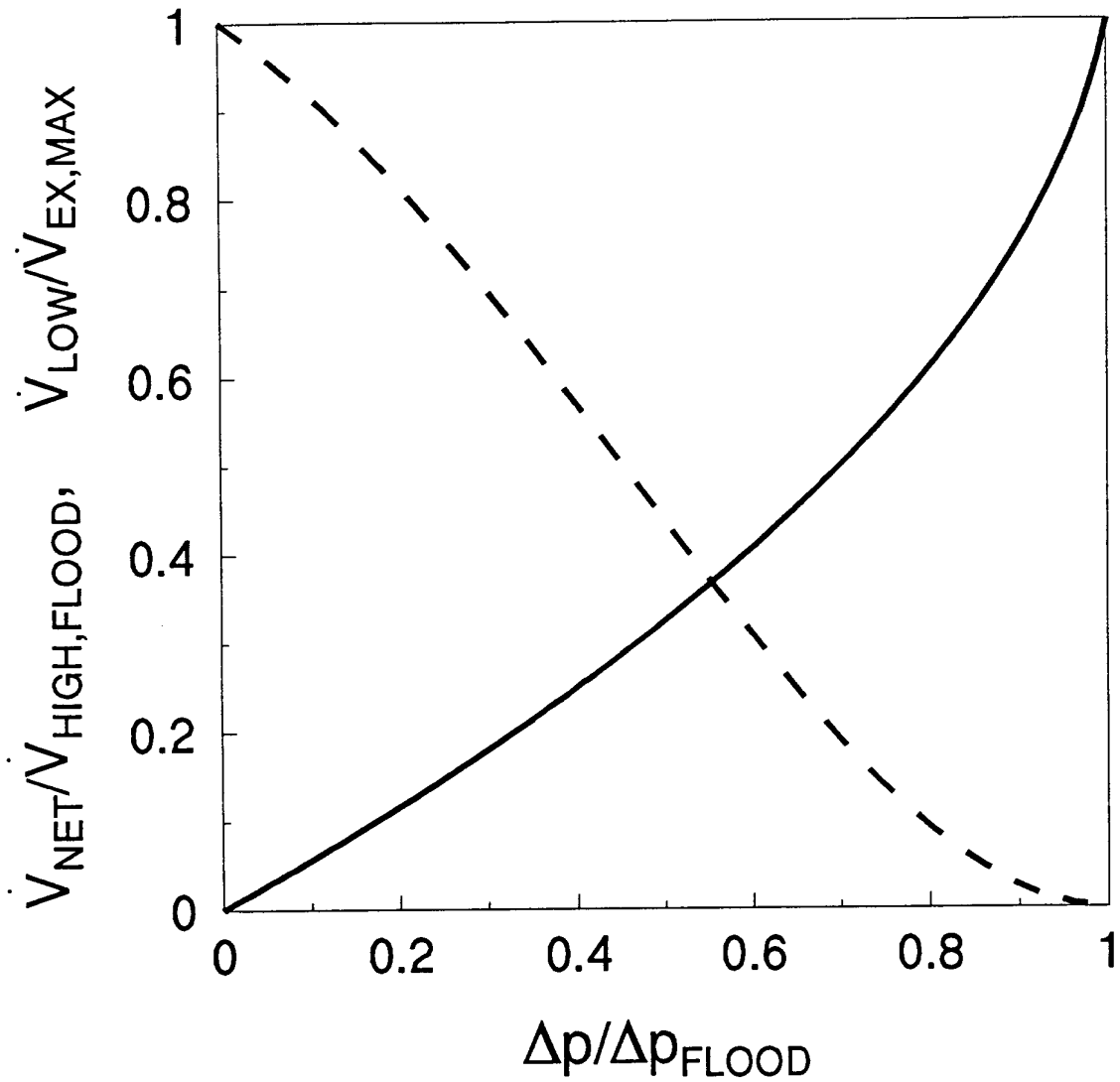


Figure 10. Plots of $\dot{V}_{\text{LOW}}^{(1)} / \dot{V}_{\text{EX, MAX}}^{(1)}$ (---) and $\dot{V}_{\text{NET}}^{(1)} / \dot{V}_{\text{HIGH, FLOOD}}^{(1)}$ (—) as functions of $\Delta p / \Delta p_{\text{FLOOD}}^{(1)}$ according to Eqs. (52), (53'), (54), and (57).

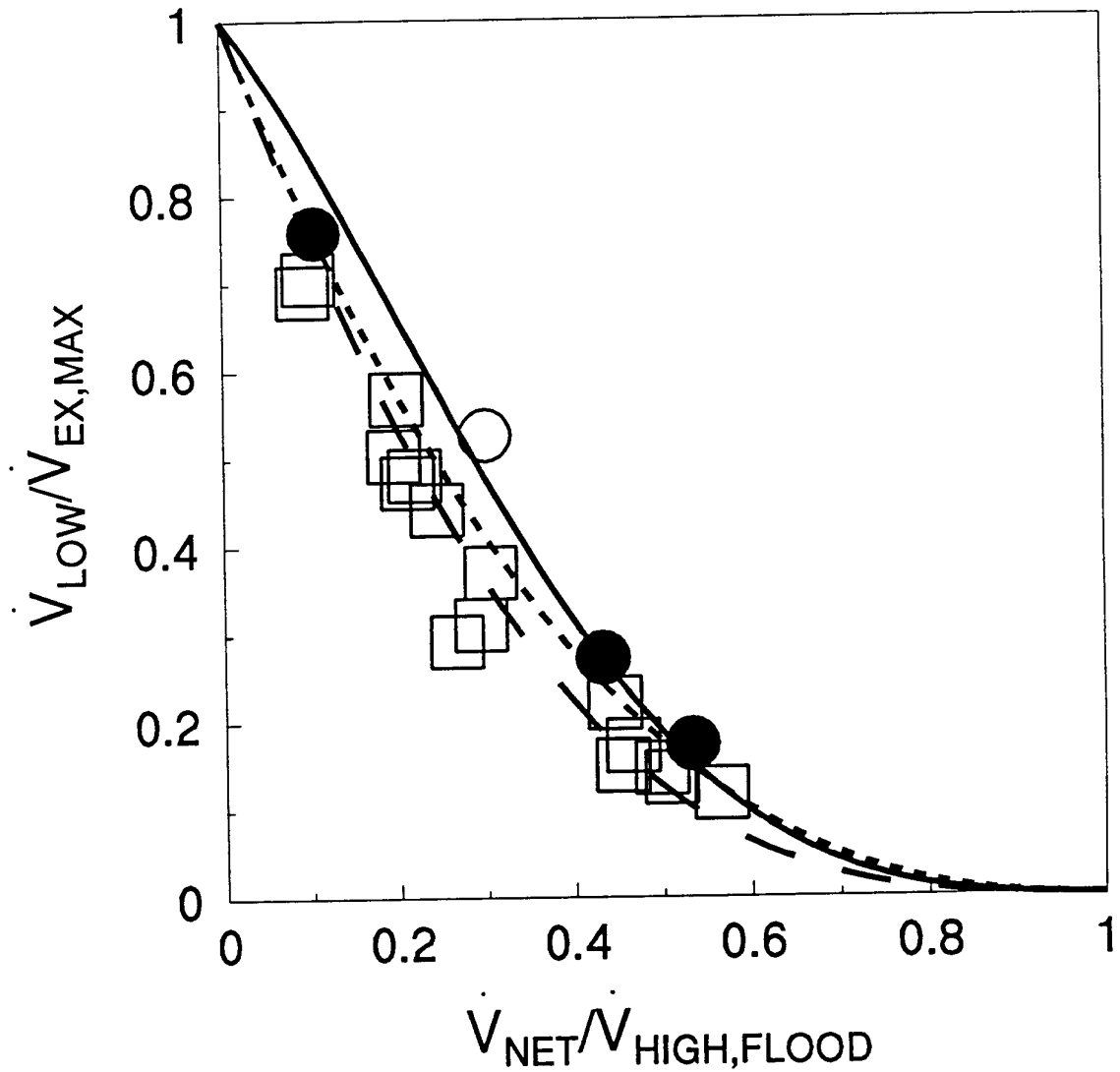


Figure 11. Plot of $\dot{V}_{LOW}^{(1)}/\dot{V}_{EX,MAX}$ as a function of $\dot{V}_{NET}^{(1)}/\dot{V}_{HIGH,FLOOD}^{(1)}$ from Eqs. (52'), (53'), (54), and (57), —; Eqs. (52'), (53'), (54), and (57'), - - -; and Eq. (60), · · ·. Plot of data of [6], i.e., Table 3 ($L/D = 0.0190$ vent, ●; $L/D = 0.113$ vent, ○; and tubes with $0.39 \leq L/D \leq 5.0$, □).

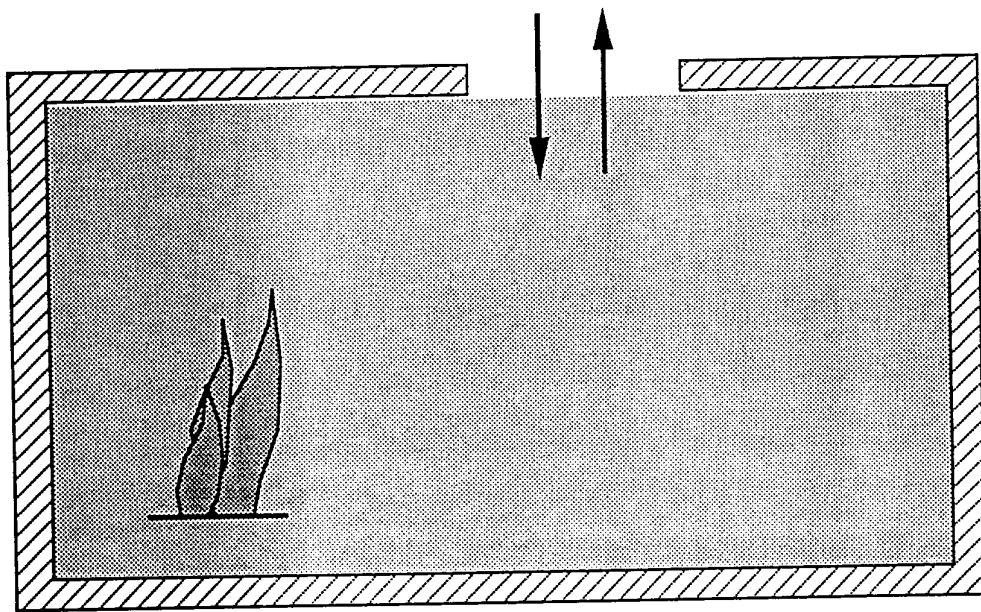


Figure 12.

Configuration of a ceiling-vented room with a fire.

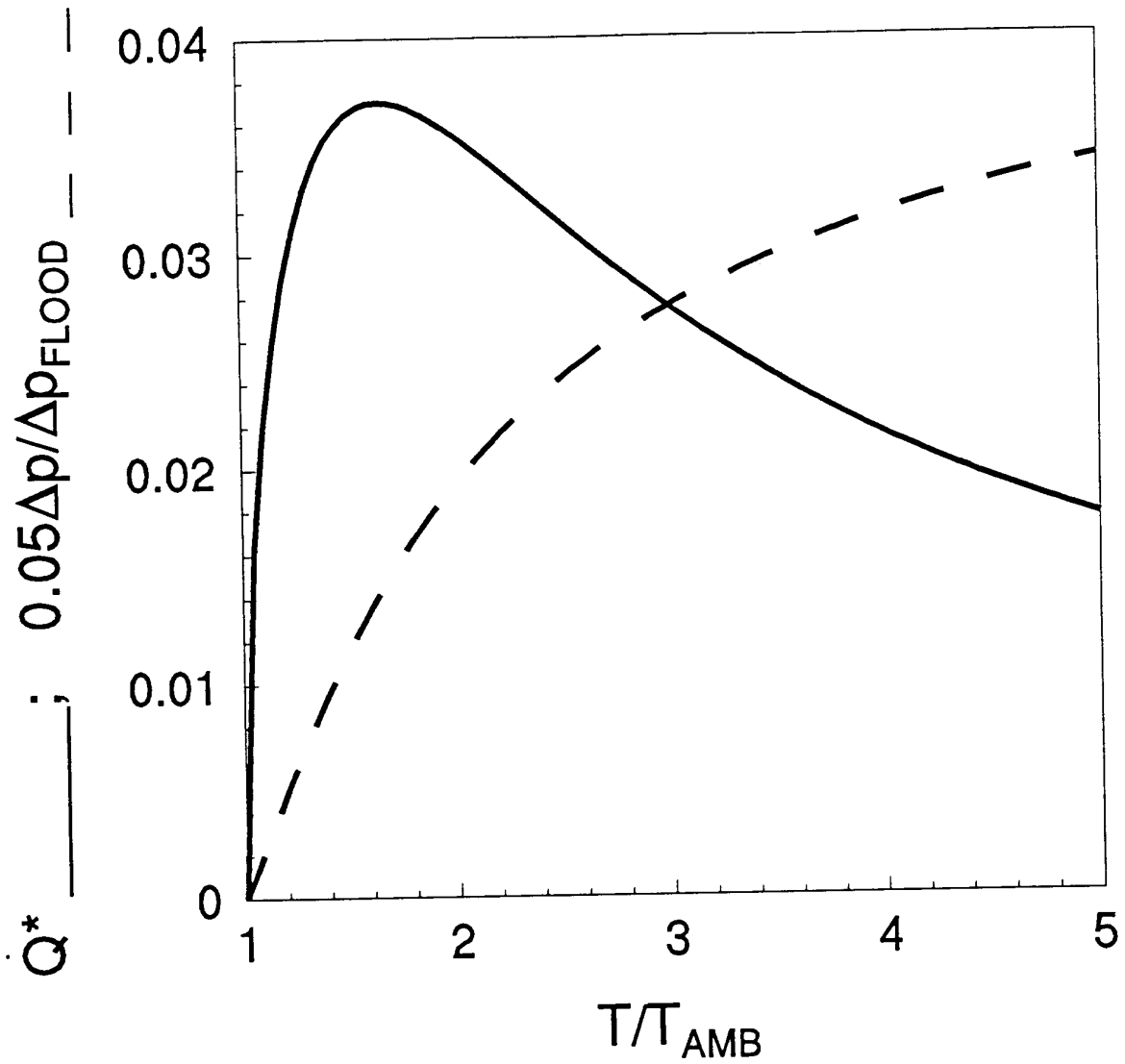


Figure 13. Plots of $\Delta p/\Delta p_{FLOOD}$ and $Q^* = Q/[(1 - \psi/\psi_{AMB})\rho_{AMB}\psi_{AMB}C_{O2}A^{5/2}g^{1/2}]$ as functions of T/T_{AMB} for the configuration of Figure 13.

NIST-114 (REV. 6-93) ADMAN 4.09	U.S. DEPARTMENT OF COMMERCE NATIONAL INSTITUTE OF STANDARDS AND TECHNOLOGY	(ERB USE ONLY) ERB CONTROL NUMBER _____ DIVISION _____ PUBLICATION REPORT NUMBER _____ CATEGORY CODE _____ NISTIR 5384
MANUSCRIPT REVIEW AND APPROVAL		PUBLICATION DATE _____ NUMBER PRINTED PAGES _____ April 1994

INSTRUCTIONS: ATTACH ORIGINAL OF THIS FORM TO ONE (1) COPY OF MANUSCRIPT AND SEND TO THE SECRETARY, APPROPRIATE EDITORIAL REVIEW BOARD.

TITLE AND SUBTITLE (CITE IN FULL)
COMBINED BUOYANCY- AND PRESSURE-DRIVEN FLOW THROUGH A SHALLOW, HORIZONTAL, CIRCULAR VENT

CONTRACT OR GRANT NUMBER _____ TYPE OF REPORT AND/OR PERIOD COVERED _____

AUTHOR(S) (LAST NAME, FIRST INITIAL, SECOND INITIAL)
 Cooper, L.Y.

PERFORMING ORGANIZATION (CHECK (X) ONE BOX)
 NIST/GAITHERSBURG
 NIST/BOULDER
 JILA/BOULDER

LABORATORY AND DIVISION NAMES (FIRST NIST AUTHOR ONLY)
Building and Fire Research Laboratory/Fire Modeling

SPONSORING ORGANIZATION NAME AND COMPLETE ADDRESS (STREET, CITY, STATE, ZIP)

PROPOSED FOR NIST PUBLICATION

<input type="checkbox"/> JOURNAL OF RESEARCH (NIST JRES)	<input type="checkbox"/> MONOGRAPH (NIST MN)	<input type="checkbox"/> LETTER CIRCULAR
<input type="checkbox"/> J. PHYS. & CHEM. REF. DATA (JPCRD)	<input type="checkbox"/> NATL. STD. REF. DATA SERIES (NIST NSRDS)	<input type="checkbox"/> BUILDING SCIENCE SERIES
<input type="checkbox"/> HANDBOOK (NIST HB)	<input type="checkbox"/> FEDERAL INF. PROCESS. STDS. (NIST FIPS)	<input type="checkbox"/> PRODUCT STANDARDS
<input type="checkbox"/> SPECIAL PUBLICATION (NIST SP)	<input type="checkbox"/> LIST OF PUBLICATIONS (NIST LP)	<input type="checkbox"/> OTHER _____
<input type="checkbox"/> TECHNICAL NOTE (NIST TN)	<input checked="" type="checkbox"/> NIST INTERAGENCY/INTERNAL REPORT (NISTIR)	

PROPOSED FOR NON-NIST PUBLICATION (CITE FULLY) _____ U.S. _____ FOREIGN _____

PUBLISHING MEDIUM
 PAPER CD-ROM
 DISKETTE (SPECIFY) _____
 OTHER (SPECIFY) _____

SUPPLEMENTARY NOTES

ABSTRACT (A 2000-CHARACTER OR LESS FACTUAL SUMMARY OF MOST SIGNIFICANT INFORMATION. IF DOCUMENT INCLUDES A SIGNIFICANT BIBLIOGRAPHY OR LITERATURE SURVEY, CITE IT HERE. SPELL OUT ACRONYMS ON FIRST REFERENCE.) (CONTINUE ON SEPARATE PAGE, IF NECESSARY.)

Combined buoyancy- and pressure-driven (i.e., forced) flow through a horizontal vent is considered where the vent-connected spaces are filled with fluids of different density in an unstable configuration (density of the top is larger than that of the bottom). With zero-to-moderate cross-vent pressure difference, Δp , the instability leads to bi-directional exchange flow between the two spaces. For relatively large Δp , the flow through the vent is uni-directional, from the high- to the low-pressure space. An anomaly of a standard vent flow model, which uses Bernoulli's equation with a constant flow coefficient, C_D , is discussed. Thus, the standard model does not predict expected bi-directional flows at small-to-moderate Δp or non-zero flow at $\Delta p = 0$. Also, when Δp exceeds the critical value, Δp_{FLOOD} , which defines the onset of uni-directional or "flooding" flow, there is a significant dependence of C_D on the relative buoyancy of the upper and lower fluids (i.e., C_D is not constant). Finally, the location of the high-pressure side of the vent, i.e., top or bottom, can be expected to influence vent flow characteristics.

Experimental data and analysis of the relevant boundary value problems are used to develop a model which removes the anomaly of the standard model and which takes all the above effects into account. The result is an algorithm, useable in zone-type fire models, to calculate flow through shallow, horizontal, circular vents under high-Grashof number conditions. The algorithm is used in example applications where steady rate-of-burning in a ceiling-vented room is estimated as a function of room temperature, vent area, and oxygen concentration. Results are consistent with available data involving ceiling-vented fire scenarios.

KEY WORDS (MAXIMUM OF 9; 28 CHARACTERS AND SPACES EACH; SEPARATE WITH SEMICOLONS; ALPHABETIC ORDER; CAPITALIZE ONLY PROPER NAMES)
 building fires; compartment fires; computer models; fire models; mathematical models; vents; zone models

AVAILABILITY <input checked="" type="checkbox"/> UNLIMITED <input type="checkbox"/> FOR OFFICIAL DISTRIBUTION - DO NOT RELEASE TO NTIS <input type="checkbox"/> ORDER FROM SUPERINTENDENT OF DOCUMENTS, U.S. GPO, WASHINGTON, DC 20402 <input checked="" type="checkbox"/> ORDER FROM NTIS, SPRINGFIELD, VA 22161	NOTE TO AUTHOR(S): IF YOU DO NOT WISH THIS MANUSCRIPT ANNOUNCED BEFORE PUBLICATION, PLEASE CHECK HERE. <input type="checkbox"/>
--	---